Eur. J. Biochem. **267**, 5313–5329 (2000) © FEBS 2000

Can yeast glycolysis be understood in terms of *in vitro* kinetics of the constituent enzymes? Testing biochemistry

Bas Teusink[1,*], Jutta Passarge[2,†], Corinne A. Reijenga[2], Eugenia Esgalhado[2], Coen C. van der Weijden[2], Mike Schepper[1], Michael C. Walsh[1,‡], Barbara M. Bakker[3], Karel van Dam[1], Hans V. Westerhoff[1,2] and Jacky L. Snoep[2]

[1]*E.C. Slater Institute, BioCentrum Amsterdam, University of Amsterdam, the Netherlands;* [2]*Department of Molecular Cell Physiology, BioCentrum Amsterdam, Faculty of Biology, Vrije Universiteit, Amsterdam, the Netherlands*

This paper examines whether the *in vivo* behavior of yeast glycolysis can be understood in terms of the *in vitro* kinetic properties of the constituent enzymes. In nongrowing, anaerobic, compressed *Saccharomyces cerevisiae* the values of the kinetic parameters of most glycolytic enzymes were determined. For the other enzymes appropriate literature values were collected. By inserting these values into a kinetic model for glycolysis, fluxes and metabolites were calculated. Under the same conditions fluxes and metabolite levels were measured.

In our first model, branch reactions were ignored. This model failed to reach the stable steady state that was observed in the experimental flux measurements. Introduction of branches towards trehalose, glycogen, glycerol and succinate did allow such a steady state. The predictions of this branched model were compared with the empirical behavior. Half of the enzymes matched their predicted flux *in vivo* within a factor of 2. For the other enzymes it was calculated what deviation between *in vivo* and *in vitro* kinetic characteristics could explain the discrepancy between *in vitro* rate and *in vivo* flux.

Keywords: metabolic control; metabolic regulation; cellular bioinformatics; glycolysis, modeling; computational biochemistry.

In the postgenomic era, all the genetic components that suffice to constitute a living organism will be known. The elucidation of the molecular function of the proteins encoded by novel genes is a major challenge in biology today [1]. Ultimately, the ambition is to understand functioning in and of the living organism from the properties of these components. The traditional biochemical approach to this 'postgenomic ambition' studies the properties of the individual components in isolation, in the belief that combining these properties afterwards will lead to a proper description of the living cell. This paper explores this promise of traditional biochemistry: can the behavior of biochemical pathways be described by combining the properties of the components in isolation?

The tenet that the behavior of the living cell can be calculated from the kinetic properties determined *in vitro*, is not undisputed. The conditions in the living cell may differ drastically from those in a test tube [2]. Regulation of the activity of enzymes by metabolites produced elsewhere in cell metabolism may be overlooked. Kinetic data obtained under different conditions cannot be combined. Enzymes that are present in a classically defined compartment may be sub-compartmented due to binding to membranes, to the cyto-skeleton or to other enzymes [2]. In addition, the concentration of enzymes in the cell is much higher than in the usual test tube experiment, a phenomenon that may be aggravated by macromolecular crowding [3–5]. It remains to be seen

Correspondence to H. Westerhoff, Department of Molecular Cell Physiology, BioCentrum Amsterdam, Faculty of Biology, Vrije Universiteit, de Boelelaan 1087, NL-1081 HV Amsterdam, the Netherlands. Fax: + 31 20 4447229, Tel.: + 31 20 4447230; E-mail: hw@bio.vu.nl

Abbreviations: AcAld, acetaldehyde; ADH, alcohol dehydrogenase; AK, adenylate kinase; ALD, fructose-1,6-bisphosphate aldolase; C-mol, mol of carbon; ENO, phosphopyruvate hydratase; F1,6bP_2, fructose-1,6-bisphosphate; F2,6bP_2, fructose 2,6-bisphosphate; F6*P*, fructose 6-phosphate; Γ, mass action ratio; Gra*P*, D-glyceraldehyde-3-phosphate; Gra*P*DH, D-glyceraldehyde-3-phosphate dehydrogenase; G3*P*DH, glycerol 3-phosphate dehydrogenase; G6*P*, glucose 6-phosphate; 1,3GriP_2, 1,3-bisphosphoglycerate; 2,3GriP_2, 2,3-bisphosphoglycerate; 2Gri*P*, 2-phosphoglycerate; 3Gri*P*, 3-phosphoglycerate; HK, hexokinase; HMP, hexose monophosphates; L-cytosol, litre of cytosolic water; PDC, pyruvate decarboxylase; PGI, phosphogluco isomerase; PFK, phosphofructokinase; PGK, phosphoglycerate kinase; PGM, phosphoglycerate mutase; PYK, pyruvate kinase; PYR, pyruvate; TPI, triosephosphate isomerase; Tps1, trehalose 6-phosphate synthase.

Enzymes: alcohol dehydrogenase (EC 1.1.1.1), adenylate kinase (EC 2.7.4.3), fructose-bisphosphate aldolase (EC 4.1.2.13), phosphopyruvate hydratase (EC 4.2.1.11), glyceraldehyde-3-phosphate dehydrogenase (phosphorylating) (EC 1.2.1.12), glycerol-3-phosphate dehydrogenase (EC 1.1.99.5), hexokinase (EC 2.7.1.1), pyruvate decarboxylase (EC 4.1.1.1), glucose-6-phosphate isomerase (EC 5.3.1.9), 6-phosphofructokinase (EC 2.7.1.11), phosphoglycerate kinase (EC 2.7.2.3), phosphoglycerate mutase (EC 5.4.2.1), pyruvate kinase (EC 2.7.1.40), triose-phosphate isomerase (EC 5.3.1.1), trehalose 6-phosphate synthase (EC 24.1.15).

**Present address*: TNO-Prevention and Health, Zernikedreef 9, 2333 CK, Leiden, the Netherlands.

†*Present address*: ARISE, University of Amsterdam, Nieuwe Achtergracht 127, 1018 WS, Amsterdam, the Netherlands.

‡*Present address*: Heineken Technical Services, Process Technology Research and Development, Burgermeester Smeetsweg 1, 2382 PH, Zoeterwoude, the Netherlands

(Received 10 February 2000, revised 30 May 2000, accepted 30 May 2000)

however, whether these considerations seriously compromise the ability to understand the functional behavior of the living cell. This paper shows how this issue can be addressed in a precise manner.

Thereby, the aim of this paper differs drastically from that of most modeling papers. Such papers aim to show that certain kinds of behavior are possible in principle, or to describe metabolic behavior, without reference to the actual molecular mechanisms. Starting out with simplified kinetic equations, they may fit the rate constants until the model reproduces the behavior of the pathway. Those models may be well suited for their specific purposes. However, for our particular aim it is necessary: (a) to employ experimentally determined enzyme kinetics, obtained from the same yeast source and measured under the same assay conditions; and (b) to refrain from adjusting kinetic parameters to obtain best fits to pathway behavior.

To examine if *in vivo* behavior may (already) be calculable from the known kinetic properties, we decided to examine the glycolytic pathway of *Saccharomyces cerevisiae* fermenting glucose. This is a metabolic pathway with a major flux in terms of its catabolism and energetics. All the relevant enzymes reside in a single compartment and have been identified and characterized both biochemically and kinetically, and the metabolite concentrations and the flux can be measured reliably.

To comply with condition (a), we collected a data set of *in vitro* kinetics of all glycolytic enzymes, largely by measuring them under one standard condition. In the same cells we gathered data on the overall behavior of the glycolytic system, i.e. fluxes and metabolite levels. We employed mathematical modeling to test whether the best available knowledge of the kinetic properties of the glycolytic enzymes allows us to understand the overall behavior of the pathway. For each enzyme we show the extent to which its *in vitro* behavior matches that *in vivo*.

EXPERIMENTAL PROCEDURES

The following paragraphs will outline the model structure. For details on rate equations of the enzymes, kinetic data and an overview of the corresponding literature the reader is referred to Appendix 1.

Stoichiometry and moiety conservation

The model includes most enzymes of the glycolytic pathway from glucose uptake to alcohol dehydrogenase (Fig. 1). When explicit kinetics were used the mass-action ratio of triosephosphate isomerase divided by the equilibrium constant was always between 0.95 and 1. Adenylate kinase (AK) should be at equilibrium when the system is at steady state, because AMP does not partake in any other reaction. The experimental levels of adenine nucleotides confirmed this within experimental error (see later). Accordingly, both triosephosphate isomerase and adenylate kinase were taken to be in equilibrium. All the other enzymes were included with explicit enzyme kinetics. In the boxes in Fig. 1 the branches are indicated that were introduced in the branched version of the model. From the reaction stoichiometries of the unbranched glycolytic pathway, three moiety conservations [6] were derived. The first corresponds to the conservation of the adenine nucleotides, the second to conservation of the nicotinamide nucleotide moiety, and the third to the conservation of oxidized compounds [7]:

$$[\mathrm{ATP}] + [\mathrm{ADP}] + [\mathrm{AMP}] = \Sigma_1 \quad (1)$$

$$[\mathrm{NAD}] + [\mathrm{NADH}] = \Sigma_2 \quad (2)$$

$$[\mathrm{BPG}] + [3\mathrm{Gri}P] + [2\mathrm{Gri}P] + [\mathrm{phospho}\textit{enol}\mathrm{pyruvate}] + [\mathrm{PYR}] + [\mathrm{AcAld}] + [\mathrm{NAD}] = \Sigma_3 \quad (3)$$

The latter conservation does not occur in the branched glycolysis model: there the pool size Σ_3 can vary (see the Results section and the discussion of the branched model below). The conservation sums Σ_i are parameters of the model.

Differential equations

The following metabolic pools were defined:

$$[\mathrm{Trio} - \mathrm{P}] = [\text{glycerone phosphate}] + [\mathrm{Gra}P] \quad (4)$$

$$P = 2[\mathrm{ATP}] + [\mathrm{ADP}] \quad (5)$$

Due to the conservation of adenine nucleotides and the equilibrium constraint on adenylate kinase, the adenine nucleotide concentrations can be described by only one free variable. The independent variable P, i.e. the sum of high-energy phosphates in adenine nucleotides, will describe the involvement of high-energy phosphate in the reactions It is related to the energy charge and the phosphorylation potential [8–10].

A set of ordinary differential equations was used to describe the time-dependence of the metabolite concentrations:

$$\mathrm{d}[\mathrm{Glc_{in}}]/\mathrm{dt} = v_{\mathrm{transport}} - v_{\mathrm{HK}} \quad (6)$$

$$\mathrm{d}[\mathrm{G6}P]/\mathrm{dt} = v_{\mathrm{HK}} - v_{\mathrm{PGI}} - 2v_{\mathrm{trehalose}} - v_{\mathrm{glycogen}}) \quad (7)$$

$$\mathrm{d}[\mathrm{F6}P]/\mathrm{dt} = v_{\mathrm{PGI}} - v_{\mathrm{PFK}} \quad (8)$$

$$\mathrm{d}[\mathrm{F1,6b}P_2]/\mathrm{dt} = v_{\mathrm{PFK}} - v_{\mathrm{ALD}} \quad (9)$$

$$\mathrm{d}[\mathrm{Trio} - \mathrm{P}]/\mathrm{dt} = 2v_{\mathrm{ALD}} - v_{\mathrm{Gra}P\mathrm{DH}}\ (-v_{\mathrm{glycerol}}) \quad (10)$$

$$\mathrm{d}[\mathrm{BPG}]/\mathrm{dt} = v_{\mathrm{Gra}P\mathrm{DH}} - v_{\mathrm{PGK}} \quad (11)$$

$$\mathrm{d}[3\mathrm{Gri}P]/\mathrm{dt} = v_{\mathrm{PGK}} - v_{\mathrm{PGM}} \quad (12)$$

$$\mathrm{d}[2\mathrm{Gri}P]/\mathrm{dt} = v_{\mathrm{PGM}} - v_{\mathrm{ENO}} \quad (13)$$

$$\mathrm{d}[\mathrm{phospho}\textit{enol}\mathrm{pyruvate}]/\mathrm{dt} = v_{\mathrm{ENO}} - v_{\mathrm{PYK}} \quad (14)$$

$$\mathrm{d}[\mathrm{PYR}]/\mathrm{dt} = v_{\mathrm{PYK}} - v_{\mathrm{PDC}} \quad (15)$$

$$\mathrm{d}[\mathrm{AcAld}]/\mathrm{dt} = v_{\mathrm{PDC}} - v_{\mathrm{ADH}}\ (-2v_{\mathrm{succinate}}) \quad (16)$$

$$\mathrm{dP}/\mathrm{dt} = -v_{\mathrm{HK}} - v_{\mathrm{PFK}} + v_{\mathrm{PGK}} + v_{\mathrm{PYK}} - v_{\mathrm{ATPase}} (-v_{\mathrm{trehalose}} - v_{\mathrm{glycogen}} - 4v_{\mathrm{succinate}}) \quad (17)$$

$$\mathrm{d}[\mathrm{NADH}]/\mathrm{dt} = v_{\mathrm{Gra}P\mathrm{DH}} - v_{\mathrm{ADH}}\ (-v_{\mathrm{glycerol}} + 3v_{\mathrm{succinate}}) \quad (18)$$

$$\mathrm{d}[\mathrm{NAD}]/\mathrm{dt} = -\ \mathrm{d}[\mathrm{NADH}]/\mathrm{dt} \quad (19)$$

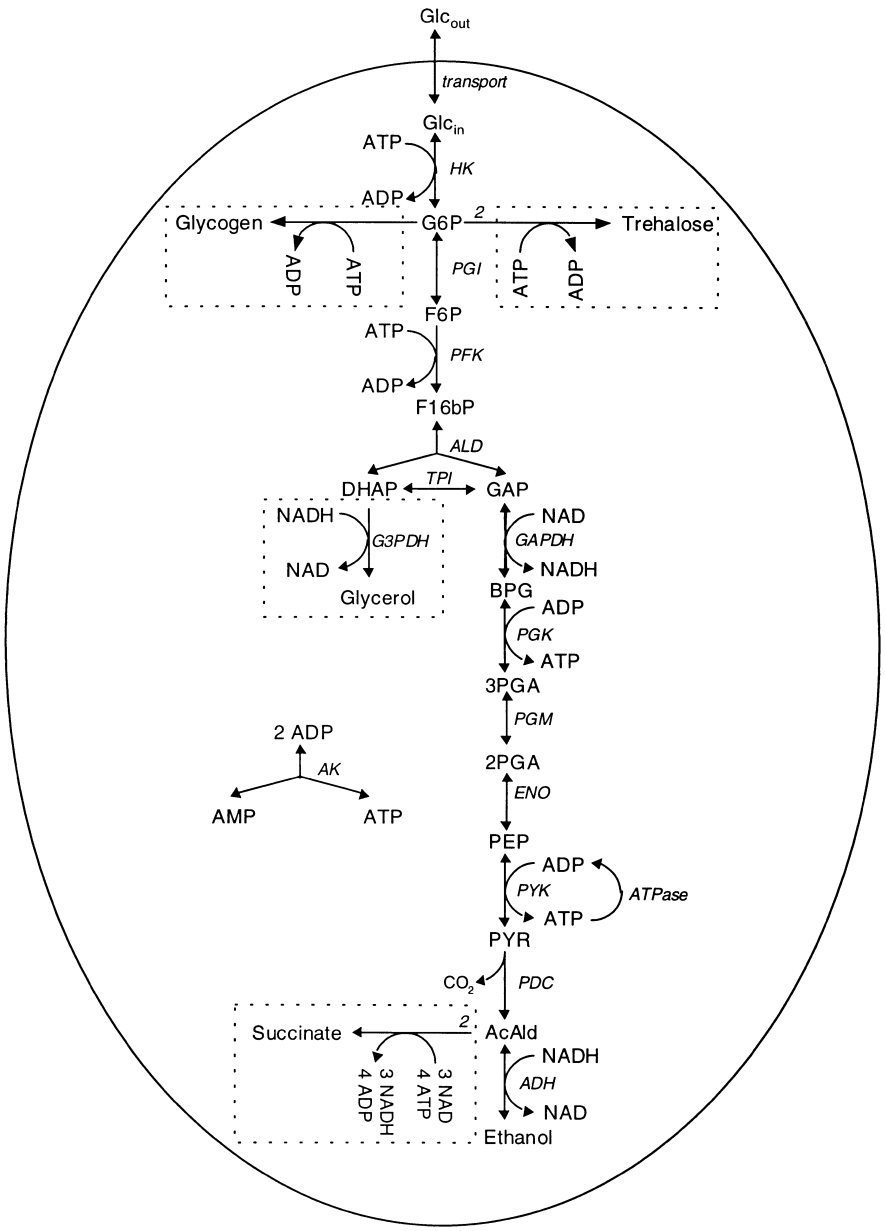

Fig. 1. Scheme of the model. Reactions in boxes show the branches introduced in the extended model. GAP, Gra*P*; DHAP, glycerone phosphate; BPG, 1,3GriP_2; 3PGA, 3Gri*P*; 2PGA, 2Gri*P*; PEP, phospho-enol-pyruvate; GAPDH, GraPDH.

The reactions in parentheses were included in the branched model only (see also Fig. 1). In the unbranched model, the acetaldehyde concentration was calculated from the changes in the concentrations of the other members of the conserved moiety Σ_3 (see Eqn. 19 for NAD). A constant concentration of 10 mM phosphate was assumed. The concentrations of the metabolites in the equilibrium pools were calculated from the pool size and the corresponding equilibrium equations [8]. For TPI:

$$K_{eq,TPI} = \frac{[Gra\mathit{P}]}{[\text{glycerone phosphate}]} \quad (20)$$

Combining Eqn (20) with Eqn (4) gives:

$$[\text{glycerone phosphate}] = \frac{[\text{Trio-P}]}{1 + K_{eq,TPI}}$$

$$[Gra\mathit{P}] = \frac{[Trio\mathit{P}]\cdot K_{eq,TPI}}{1 + K_{eq,TPI}} \quad (21a, b)$$

For the adenine nucleotides the equilibrium equation is as follows:

$$K_{eq,AK} = \frac{[AMP][ATP]}{[ADP]^2} \quad (22)$$

Solving Eqns (1), (5) and (22) for the three unknowns gives two solutions for [ATP], of which only one yields physiologically relevant ATP concentrations [10]:

$$[ATP] = \frac{-b + \sqrt{b^2 - 4ac}}{2a} \quad (23)$$

with

a=1-4$K_{eq,AK}$

b=$\sum_1$−P(1 − 4$K_{eq,AK}$)

c= − $K_{eq,AK}P^2$

Table 1. Experimental determination of fluxes and metabolite concentrations in compressed Koningsgist challenged with 100 mm glucose (averages and SEM; n = 3). The trehalose and glycogen fluxes are expressed in units of glucose. See Materials and methods for details.

Fluxes	Rate (mmol·min^{-1}·L-cytosol^{-1})	Rate[a] (U·mg protein^{-1})
Glucose	108 ± 1.6	0.40
Ethanol	135 ± 3.2	0.50
CO_2	154 ± 3.4	0.57
Glycogen	6.0 ± 0.4	0.022
Trehalose	4.8 ± 1.2	0.018
Glycerol	18.2 ± 1.3	0.068
Succinate	2.9 ± 0.2	0.011
Pyruvate	2.2 ± 0.8	0.008
Acetate	0.5 ± 0.3	0.002
Metabolites	**concentration (mmol·L-cytosol^{-1})**	
G6*P*	2.45 ± 0.14	
F6P	0.62 ± 0.02	
F1,6bP_2	5.51 ± 0.04	
Glycerone phosphate	0.81 ± 0.01	
Gly3P	0.15 ± 0.10	
3Gri*P*	0.90 ± 0.02	
2Gri*P*	0.12 ± 0.01	
Phospho*enol*pyruvate	0.07 ± 0.00	
Pyruvate	1.85 ± 0.64	
Acetaldehyde	0.17 ± 0.02	
ATP	2.52 ± 0.20	
ADP	1.32 ± 0.10	
AMP	0.25 ± 0.07	
NAD	1.20 ± 0.13	
NADH	0.39 ± 0.09	

[a] Included for comparison with specific activities of Table 3.

The concentrations of ADP and AMP follow from Eqns (12) and (1), respectively.

The differential equations were integrated on a personal computer using the metabolic modeling software SCAMP [11].

Measurement of enzyme kinetics

Compressed yeast (Koningsgist, DSM Bakery Ingredients) was used in all experiments. Glucose transport was measured for intact cells resuspended in 100 mM KH_2PO_4 buffer, pH 6.5, as described by [12]. To measure the kinetics of intracellular enzymes (except for PFK and PYK), 1 g of yeast was resuspended in 1 mL of ice-cold Millipore water. The suspension was diluted 20 times with 20 mM KH_2PO_4, pH 7.0, containing 1 mM of the protease inhibitor phenylmethanesulphonyl fluoride. Acid-washed glass beads (1 g, 0.4–0.5 mm diameter) were added to 1 mL of cell suspension in an Eppendorf tube. The mixture was shaken for 15 min at 4 °C. The extract was centrifuged (Eppendorf centrifuge, 15 min, maximal speed) at 4 °C and the supernatant was stored on ice until further use. For each enzyme to be characterized, the extract was diluted into 20 mM KH_2PO_4, pH 7.0, until the enzyme activity was proportional to the enzyme concentration. All enzyme assays were carried out in 50 mM Pipes buffer of pH 7.0 containing 100 mM of KCl, 5 mM of $MgSO_4$ plus specific additions to be specified below. A COBAS BIO (Roche, Basel) automated analyzer was used for spectroscopic measurement of the metabolite concentrations through NAD(P)H-linked assays.

Hexokinase was measured with 0.2 mM NADP, 2.8 U·mL^{-1} glucose 6-phosphate dehydrogenase, and ATP and glucose at varying concentrations. Phosphoglucose isomerase was measured in the forward direction in the presence of 0.15 mM NADH, 1 mM ATP, 12.5 U·mL^{-1} phosphofructokinase, 1.5 U·mL^{-1} aldolase, 50 U·mL^{-1} triosephosphate isomerase and 4.3 U·mL^{-1} glycerol 3-phosphate dehydrogenase, with glucose 6-phosphate as the substrate. For the reverse reaction, 0.2 mM NADP and 2.8 U·mL^{-1} glucose 6-phosphate dehydrogenase was used, with fructose 6-phosphate as the substrate. Aldolase was assayed with 0.15 mM NADH, 50 U·mL^{-1} triosephosphate isomerase and 4.3 U·mL^{-1} glycerol 3-phosphate dehydrogenase, with fructose-1,6-bisphosphate as the substrate. Glyceraldehyde-3-phosphate dehydrogenase was measured in the reverse direction with 1 mM ATP, 0.9 mM EDTA, 0.2 mM dithioerythritol, 0.15 mM NADH, 50 U·mL^{-1} phosphoglycerate kinase, with 2 mM 3-phosphoglycerate as the substrate (therefore only the V_{max} was measured). Phosphoglycerate kinase was measured in the reverse reaction in the presence of 0.9 mM EDTA, 0.15 mM NADH, 1 mM ATP and 8 U·mL^{-1} glyceraldehyde-3-phosphate dehydrogenase, with 3-phosphoglycerate as the substrate. Phosphoglycerate mutase was assayed in 0.15 mM NADH, 1 mM ADP, 0.5 mM glycerate 2,3-bisphosphate, 0.9 mM EDTA, 2.8 U lactate dehydrogenase, 7 U·mL^{-1} pyruvate kinase, 3 U·mL^{-1} enolase, with 3-phosphoglycerate as the substrate. Enolase was measured with 0.15 mM NADH, 1 mM ADP, 0.9 mM EDTA, 14 U·mL^{-1} lactate dehydrogenase, 7 U·mL^{-1} pyruvate kinase, with 2-phosphoglycerate as the substrate. Pyruvate decarboxylase was assayed with 5 mM $MgCl_2$ (replacing the $MgSO_4$

of the assay buffer), 0.2 mM thyaminepyrophosphate, 15 mM NADH, 110 U·mL^{-1} alcohol dehydrogenase, with pyruvate as the substrate. Alcohol dehydrogenase was assayed in the reverse direction with 1 mM of oxidized glutathione, 10 mM semicarbazide and 2 mM NAD with ethanol as the substrate. For pyruvate kinase, cells were extracted with glass beads in 100 mM Pipes buffer of pH 7.0 containing 10 mM KCl and 1 mM phenylmethanesulfonyl fluoride. The assay contained 70 mM Pipes buffer at pH 7.0, 100 mM KCl, 1 mM $MgCl_2$, 0.2 mM NADH, 10 U·mL^{-1} lactate dehydrogenase and ADP and phospho*enol*pyruvate as variable substrates. The effect of fructose-1,6-bisphosphate on the kinetics of pyruvate kinase was tested in a concentration range from 0.025 to 5 mM.

For measurement of phosphofructokinase kinetics, the enzyme was partly purified from a cell-free extract. The extract was prepared in extraction buffer containing 40 mM of Mes, 100 mM KCl, 1 mM $MgCl_2$, 2 mM fructose 6-phosphate, 50 mM KH_2PO_4, 1 mM phenylmethanesulfonyl fluoride and 5 mM β-mercaptoethanol at pH 6.4. To 25 g yeast in 5 mL buffer, 25 g of glass beads was added and the cells were broken in a CO_2 cooled homogenizer (Braun). The extract was centrifuged and phosphofructokinase in the supernatant was purified by ammonium sulfate precipitation and Sephadex G200 chromatography using an eluent buffer containing 40 mM of Mes, 100 mM KCl, 1 mM $MgCl_2$, 0.2 mM ATP, 25 mM KH_2PO_4 and 5 mM mercaptoethanol at pH 6.8. The assay contained 70 mM Pipes buffer at pH 7.0, 90 mM KCl, 10 mM $MgSO_4$, 15 mM KH_2PO_4, 10 mM NH_4Cl, 0.15 mM NADH, 1.5 U·mL^{-1} aldolase, 13.5 U·mL^{-1} triosephosphate isomerase and 2.5 U·mL^{-1} glycerol 3-phosphate dehydrogenase. The coupling enzymes had been desalted over a PD10 column (Pharmacia). F6*P*, ATP, AMP and F2,6P_2 were used at various concentrations as substrates or effectors.

Experimental determination of metabolites and fluxes in the intact cells

Compressed yeast (Koningsgist), was resuspended in potassium phosphate buffer (100 mM, pH 6.5). It was then mixed with prewarmed (30 °C) and nitrogen-fluxed phosphate buffer to a final concentration of 50 (g cake)·L^{-1} (which was 5–6 g·L^{-1} protein, using Lowry's protein assay [13] with BSA as a standard). Glucose was added to a final concentration of 100 mM and samples were withdrawn at regular time-intervals and quenched in ice-cold perchloric acid or −40 °C methanol, depending on the metabolites to be measured. Most metabolites were measured in 5% (final concentration) perchloric acid extracts (G6*P*, F6*P*, F1,6bP_2, glycerone phosphate, NAD, ATP, ADP and AMP), which was also used to measure the pathway substrates and products glucose, ethanol, glycerol, pyruvate, acetate and succinate. Such extracts were neutralized with potassium carbonate and assayed for the metabolites by enzymatic analyses according to Bergmeyer [14], as reported previously [15,16]. Intracellular pyruvate, phospho*enol*-pyruvate, 2Gri*P*, 3Gri*P*, NAD and NADH were measured after quenching metabolism in cold methanol, which allows removal of the extra-cellular medium and concentration of the sample. After centrifugation of the methanol-quenched cells, NADH was measured by alkaline extraction of the pellet according to [17]; the other metabolites were extracted with perchloric acid and analyzed as described [16]. Cytosolic metabolite concentrations were calculated by a conversion factor of 3.75 mL of cell water per gram protein [16,18].

Metabolites, glucose, acetate and succinate were measured by enzymatic analysis; ethanol and glycerol were measured by HPLC (Aminex 87H column from Biorad, 55 °C mobile phase 0.01 N H_2SO_4 at 0.5 mL·min^{-1}, refraction index detector 131 from Gilson). Glycogen and trehalose were determined by the method of [19], Acetaldehyde was determined by rapid filtration immediately after taking a sample, as described [20]. Equilibration of intracellular and extracellular acetaldehyde was assumed. Carbon dioxide production was measured by off-gas analysis using mass spectrometry (VG gas analysis systems Ltd, type MM8–80), calibrated to air of known composition.

RESULTS

The intact cell: measured fluxes and metabolite concentrations

We monitored glucose consumption and product formation for 45–60 min after addition of 100 mM of glucose to resuspended compressed yeast. Some fluxes showed more complex behavior, especially the net flux into trehalose, which was negative at first but became positive after some 20 min (Fig. 2C). The concentration of CO_2 in the off-gas increased during the first 20 min after glucose addition. This was probably due to equilibration of the buffer with bicarbonate and the filling of the head space of the fermentor. It then

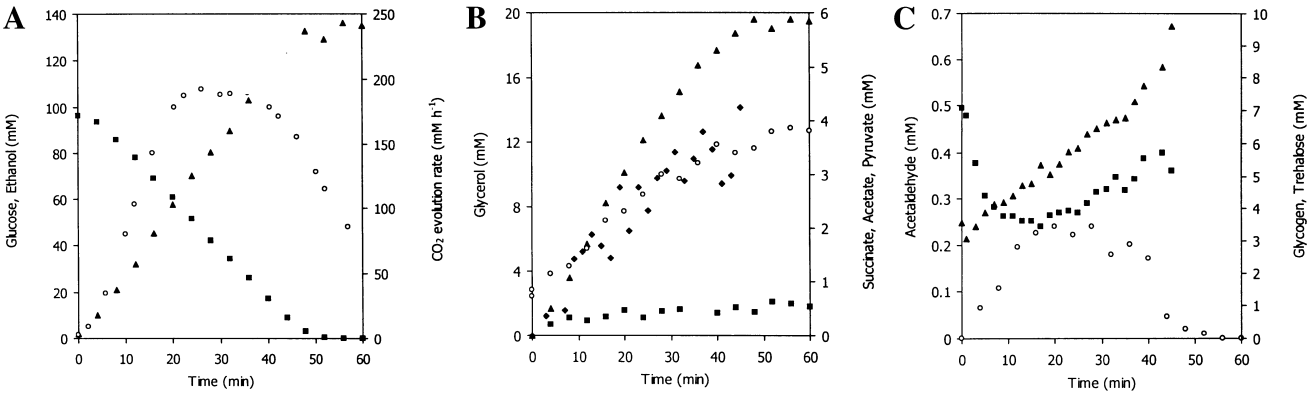

Fig. 2. External concentrations and CO_2 flux during anaerobic glucose fermentation in resting yeast. (A) glucose (■), ethanol (▲) and CO_2 evolution rate (○). (B) glycerol (▲), succinate (○), acetate (■) and pyruvate (◆). (C) glycogen (▲), trehalose (■) and acetaldehyde (○). Glycogen and trehalose are expressed in units of glucose.

Table 2. Kinetic parameters used in the model. The rate equations used for each enzyme and the source of the parameter values are given in Appendix 1. For equations and meanings of the symbols regarding PFK, see Appendix 2.

Enzyme	K_a (mM)	K_b (mM)	K_p (mM)	K_q (mM)
Glc transport	1.19 (Glc_{out})		1.19 (Glc_{in})	
Int. const. K_i	0.91			
HK	0.08 (Glc_{in})	0.15 (ATP)	30 (G6*P*)	0.23 (ADP)
PGI	1.4 (G6*P*)		0.3 (F6*P*)	
ALD	0.3 (F1,6bP_2)		2.4 (glycerone phosphate)	2.0 (Gra*P*)
K_i				10 (Gra*P*)
Gra*P*DH	0.21 (Gra*P*)	0.09 (NAD)	9.8×10^{-3} (1,3GriP_2)	0.06 (NADH)
PGK	3×10^{-3} (1,3GriP_2)	0.2 (ADP)	0.53 (3Gri*P*)	0.3 (ATP)
PGM	1.2 (3Gri*P*)		0.1 (2Gri*P*)	
ENO	0.04 (2Gri*P*)		0.5 (phospho*enol*pyruvate)	
PYK	0.14 (phospho*enol*pyruvate)	0.53 (ADP)	21 (Pyr)	1.5 (ATP)
PDC	4.33 (Pyr)			
Hill coefficient	1.9			
ADH	17 (EtOH)	0.17 (NAD)	0.11 (NADH)	1.11 (AcAld)
K_i	90 (EtOH)	0.92 (NAD)	0.031 (NADH)	1.1 (AcAld)
G3*P*DH	0.4 (glycerone phosphate)	0.023 (NADH)	1 (G3P)	0.93 (NAD)
PFK	K_R (mM)	c	K (mM)	c_i
F6*P*	0.1	0		
ATP	0.71	3	0.65	100
AMP			0.0995	0.0845
F1,6bP_2	–	–	0.111	0.397
F2,6bP_2			6.82×10^{-4}	0.0174
Others	5.12 (g_R)	1 (g_T)	0.66 (L_0)	

became constant for 20 min and decreased subsequently as the glucose in the medium ran out. After 20 min all fluxes had reached a steady state, as had the metabolite concentrations (although some metabolite concentrations still showed time-dependencies in the order of 20% of the average concentration). The rates and metabolite levels summarized in Table 1, are averages over the period from 20 to 40 min after glucose addition.

Although most of the glucose is converted into ethanol and CO_2, a significant proportion of the glucose-derived carbon was directed to the branches of glycolysis (Table 1). These include glycogen, trehalose, glycerol and succinate. Small amounts of acetate and pyruvate were found (Fig. 2B). One mol of succinate derived from 1 mol of glucose (with the release of two moles of CO_2) produces 5 mol of NADH [21]. The production of succinate can account for 80% of the glycerol formed during the glucose fermentation; together with the acetate and pyruvate produced, for 95%.

The rate of CO_2 production was higher than can be accounted for by the rates of ethanol and succinate production. We assume that the difference is caused by loss of ethanol (and possibly acetaldehyde) via the off-gas. If 1 mol of glucose is taken to produce 2 mol of CO_2, the carbon balance was met for 90%.

Enzyme kinetics and displacement from equilibrium

The literature data on enzyme kinetics had mostly been determined under experimental conditions different from those of our intact-cells experiment. Therefore we determined a number of kinetic parameters in an extract of the cells also used for the flux and metabolite measurements. The literature was perused to select the best assay, to determine the kinetic mechanism, to prevent pitfalls and to complement our own data set. Table 2 gives the resulting parameter set (cf. Appendix 1). In Table 3 the maximum forward rate, the equilibrium constant and the displacement from equilibrium is given for each step, using the experimentally determined metabolite concentrations and the equilibrium constants. Because no data on the intracellular glucose concentration was available for the condition analyzed here, the glucose transport step was lumped with the hexokinase step. Because 1,3-bisphosphoglycerate is unstable and its concentration is too low to be measured accurately, the same was performed for the enzymes Gra*P*DH and PGK. The steps close to equilibrium were PGI, the combined Gra*P*DH-PGK step and PGM. The transport-HK step, PFK, and PYK were virtually irreversible. Also enolase and aldolase were quite far from equilibrium.

Model results: unbranched glycolysis

Arguing that for nongrowing cells the flux through the branches is relatively small, we first modeled without the branch reactions. Using the experimentally determined metabolite levels, the three conserved moieties (Σ_1, Σ_2 and Σ_3, Eqns. 1–3) were calculated at 4.1, 1.6 mM, and 4.3 mM, respectively. Using these moiety-conserved sums, the parameter values given in Tables 2 and 3, and the experimental steady-state concentrations of the metabolites as initial conditions (Table 1), we numerically integrated the differential equations. No steady state was reached.

Inspection of the time course of the simulation showed that F1,6bP_2, Gra*P* and glycerone phosphate were increasing to extremely high levels, whereas the other metabolites reached a constant level. The flux through the enzymes upstream F1,6bP_2 became constant at 0.48 C-mol·min^{-1}· L-$cytosol^{-1}$;

Table 3. Experimentally determined maximal rates, equilibrium constants from literature (as specified in the last column) and displacement from equilibrium for each step in the model. Maximal rates are expressed as U (i.e. μmol·min^{-1}) per mg total protein. For aldolase the unit of the equilibrium constant is mM^{-1}. For Gra*P*DH, [phosphate] was taken 10 mM. In cases where protons are involved, the concentration of H^+ was taken to be 10^{-7} M (pH 7.0). Γ is the mass-action ratio ([products]/[substrates]), based on the steady-state metabolite concentrations of Table 1.

Enzyme	V_{max} (U·mg protein^{-1})	K_{eq}	Γ/K_{eq}	Reference
Glc transport	0.36	1		[120]
HK	0.84	3.8×10^3	6.8×10^{-6} [a]	
PGI	1.26	0.314	0.81	[121]
PFK	0.68	8.0×10^2	5.8×10^{-3}	[122]
ALD	1.19	0.069	0.078	[14]
TPI	8.4	0.045	1	[14]
GraPDH	4.4/24.3 [b]	0.0056	0.88 [c]	[81]
PGK	4.8 [d]	3.2×10^3		[14]
PGM	9.4	0.19	0.70	[88]
ENO	1.35	6.7	0.087	[14]
PYK	4.05	6.5×10^3	7.8×10^{-3}	[14]
PDC	0.65			
ADH	3.0 [d]	1.45×10^4	0.53	[123]
AK		0.45	0.80	[14]
G3PDH		4.3×10^3	1.3×10^{-4}	[14]

[a] Combined mass action and equilibrium constant of glucose transport and hexokinase. The equilibrium constant of hexokinase was calculated from standard thermodynamic properties of the reactants from [124]. [b] The V_{max} for the forward and reverse reaction are given, respectively. [c] Combined mass action and equilibrium constant of Gra*P*DH and PGK. [d] For PGK and ADH the V_{max} for the reverse reaction was measured. For ADH the equilibrium constant is also defined in the reverse reaction (acetaldehyde and NADH being the products).

the flux through the enzymes downstream Gra*P* at only 0.38 C-mol·min^{-1}·L-cytosol^{-1} (where C-mol is a mol of carbon and L-cytosol is a litre of cytosolic water), explaining the accumulation of the metabolites in between. This failure of the 'lower' part of glycolysis to keep up with the flux through the 'upper' part is reminiscent of the phenotype seen in mutants in trehalose 6-phosphate synthase (Tps1) which has been understood from the negative feedback of Tps1 on hexokinase [22–24] and Appendix 1. The appearance of a '*tps1Δ*-phenotype' depends on some limitation in the lower part of glycolysis [24]. This limitation can be understood by considering the moiety conservation of the oxidized species in the lower part of glycolysis (Eqn. 3). Given the *in vitro* kinetics of PDC, the pyruvate concentration that is required to accommodate a flux of 0.48 C-mol·min^{-1}·L-cytosol^{-1}, is 8 mM. This is higher than the conserved sum of oxidized compounds, Σ_3, which was 4.3 mM. Consequently, the flux through PDC could not reach the 0.48 C-mol·min^{-1}·L-cytosol^{-1} required to reach a steady state. F1,6bP_2, glycerone phosphate and Gra*P* accumulated, because their concentrations were not restrained by Σ_3, and because PFK was not sensitive to its product F1,6bP_2 (see Discussion and Appendix 2).

A 6.1-fold increase in the V_{max} of PDC was required to obtain a stable steady state with the experimentally determined concentration of pyruvate (Table 4). The glucose consumption rate of 88 mmol·min^{-1}·L-cytosol^{-1} was some 20% lower than the measured value of 108 mmol·min^{-1}·L-cytosol^{-1}. Most of the calculated metabolite levels did not differ by more than a factor of two from the experimental values. Exceptions were F6*P*, F1,6bP_2 and NADH.

Is the correspondence between *in vitro* kinetics and *in vivo* behavior improved by considering the branches of glycolysis?

An alternative explanation for the failure of the original *in vitro* kinetics to describe the *in vivo* situation could be that the branches from glycolysis were ignored. The kinetics of the enzymes of most branches has not been characterized well. Because we focus on steady state, the branches into trehalose and glycogen could just as well be introduced as constant rates and did therefore not require additional parameter estimation. This was not possible for the glycerol and the succinate branch, because allowing a temporal variation in these rates (by not fixing them as constants, but making them concentration-dependent) leads to adjustment of the redox state and hence, introduction of these branches relieves the moiety conservation of oxidized species (Σ_3).

Even with the maximal rate of PDC kept at its original, empirical, level, the branched model attained a stable steady state (Table 4). Apparently, the glycerol and succinate branches relieved the moiety conservation of oxidized compounds, so that the increased pyruvate concentration did not dwindle the NAD concentration; Gra*P*DH could reach the rate required for a steady state. As expected from the low fluxes through the branches, the metabolite levels were only somewhat lower and more displaced from the empirical values than in the unbranched case. Thus, including the branches did lead to a substantial qualitative improvement of the model in the sense that now a steady state was reached with the original *in vitro* determined parameter set. It did not, however, lead to a better correspondence between model prediction and experiment than including an increased activity of PDC in the unbranched version of the model.

Assessing the difference between in vitro and in vivo kinetics for the glycolytic enzymes

The *in vitro* determined kinetic parameters of the glycolytic enzymes did not enable us to calculate properly all the *in vivo* concentrations of glycolytic metabolites. Is the *in vitro* biochemistry for all enzymes remote from their *in vivo* behavior, or is there just a discrepancy for one or two enzymes?

Table 4. Model predictions of steady-state fluxes k_{ATPase} and metabolite concentrations in the unbranched and branched model. Concentrations of glucose and ethanol were fixed at 50 mM. In both models, k_{ATPase} was tuned to obtain the measured ATP concentration of 2.5 mM (i.e. $k_{ATPase} = 70$ min^{-1} and $k_{ATPase} = 33.7$ min^{-1}, respectively). In the unbranched model, the maximal rate of PDC was adjusted to obtain the experimentally obtained concentration of pyruvate (1.85 mM). Without this adjustment, no steady state was reached (see text for explanation). In the branched model, the V_{max} of G3PDH was tuned to yield the measured glycerol flux (i.e. V_{max}, G3PDH = 0.26 U·mg protein^{-1}) and $k_{succinate}$ was adjusted to obtain the measured concentration of acetaldehyde of 0.17 mM (i.e. $k_{succinate} = 21.4$ min^{-1}).

Fluxes	Unbranched model rate (mmol·min^{-1}·L-cytosol^{-1})	Branched model rate (mmol·min^{-1}·L-cytosol^{-1})
Glucose	88	88
Ethanol	176	129
Glycogen		6.0
Trehalose		4.8
Glycerol	–	18.2
Succinate	–	3.6
Metabolites	**Concentration (mmol·L-cytosol^{-1})**	**Concentration (mmol·L-cytosol^{-1})**
G6*P*	1.51	1.07
F6*P*	0.16	0.11
F1,6bP_2	0.98	0.60
Glycerone phosphate	0.95	0.74
3Gri*P*	0.52	0.36
2Gri*P*	0.07	0.04
Phospho*enol*pyruvate	0.08	0.07
Pyruvate	1.85	8.52
Acetaldehyde	0.24	0.17
ATP	2.52	2.51
ADP	1.29	1.29
AMP	0.30	0.30
NAD	1.55	1.55
NADH	0.04	0.04

From the experimental flux and the reaction stoichiometries, one can readily deduce the steady-state rate of each enzyme. For most enzymes the concentrations of all its substrates, products and metabolic modifiers were measured as well. For these enzymes one can therefore calculate by how much one would have to change the magnitude of any of the parameters in order for the rate and concentrations to satisfy the rate equation.

Here we refrain from deciding *a priori* that the intracellular amount of enzyme [25,26] was at fault. Rather, we asked for each enzyme, by how much we would have to change: (a) The $V_{max\ forward}$ and $V_{max\ reverse}$ concomitantly (i.e. the intracellular activity of the enzyme); (b) the equilibrium constant (through changing the maximal reverse rate, leaving all other kinetic constants unchanged); (c) the substrate/product affinities

Table 5. Required adjustments to V_{max}, K_{eq} or pairs of Michaelis–Menten constants for each enzyme to fit the flux and measured metabolite concentrations for the branched model. Numbers give the dimensionless factor by which the original parameter had to be multiplied. Equating the rates of glucose transport and hexokinase resulted in a combined equation for the rate through these two steps as a function of the concentration of external glucose, ATP, ADP and glucose 6-phosphate only. –, Not calculated; NS, no solution.

Enzyme	V_{max}	K_{eq}	K_a/K_p	K_b/K_q	K_p/K_q
HXT	1.2	–	NS	–	–
HK	NS	NS	NS	NS	NS
PGI	4.1	3.8	NS	–	–
PFK	0.73	–	–	–	–
ALD[a]	0.35	0.12	28	37	109
PGM	1.0	1.0	0.96	–	–
ENO	0.73	0.26	11	–	–
PYK[b]	1.1	NS	0.89	0.65	1.4
PDC[c]	6.1	–	NS	–	–
ADH	0.11	6.0	–	–	–

[a] K_a/K_p corresponds to F1,6bP_2 and Gra*P*; K_b/K_q corresponds to F1,6bP_2 and glycerone phosphate; K_p/K_q corresponds to Gra*P* and glycerone phosphate, where K_p should be multiplied and K_q divided by the indicated factor. [b] K_a, K_b, K_p and K_q correspond to phospho*enol*pyruvate, ADP, Pyr and ATP, respectively. For K_p/K_q K_p should be multiplied and Kq divided by the indicated factor. [c] K_a/K_p stands for the $K_{0.5}$ of pyruvate only.

(equally, keeping the equilibrium constant unchanged; when two substrates and two products were present, either the K_m values for the structurally related substrate and product were changed in pairs, or those of two reactants whose affinities were most uncertain).

Changes in affinity constants did not always lead to a solution within the constraints of the Haldane relationship. Where a solution was found, however, the changes required were generally much larger than for the limiting rate or the equilibrium constant (Table 5). For half of the enzymes the *in vitro* V_{max} values needed adjustment by less than a factor of two for the model to predict the *in vivo* rate at the experimentally determined metabolite levels (Table 5). By contrast, alcohol dehydrogenase appeared nine times more active *in vitro* than it should be *in vivo*. The V_{max} of PDC had to be increased some sixfold; changes in its other parameters did not lead to a solution. The kinetics of PGI had to be changed some fourfold, either by an increase in its maximal rate or by increasing its equilibrium constant. Aldolase required a threefold reduction in its limiting rate, or an eightfold decrease in its equilibrium constant. The V_{max} of glucose uptake was 10% lower than the flux through that step. Consequently, no solution was found for any kinetic parameter in the transport-HK module except for the maximal rate of glucose transport.

The solution for the Gra*P*DH/PGK module was more complicated because of the uncertainty in the concentration of 1,3GriP_2. The overall equilibrium constant is about 17, at pH 7 and a phosphate concentration of 10 mM. The mass action ratio of the substrates and the products of this combined step was close to the overall equilibrium constant (Table 3). Consequently, both reactions must be close to equilibrium for both reactions to proceed in the forward (glycolytic) direction. With the known kinetics of Gra*P*DH, no concentration of 1,3GriP_2 could be found that lead to the required flux through the enzyme. With the kinetics of PGK, the concentration of 1,3GriP_2 required to match the flux exceeded the concentration allowing the Gra*P*DH reaction to proceed in the glycolytic direction. Simultaneous adjustment of kinetic parameters of both enzymes was examined for the case where both enzymes were equally displaced from equilibrium, i.e. at [1,3GriP_2] = 5.83×10^{-4} mM. For Gra*P*DH, the V_{max} in both directions required a 23-fold increase, or a 2.58-fold increase for the V_{max} in the forward direction only; the latter adjustment changes the equilibrium constant. Other parameter changes did not lead to a solution. For PGK, the V_{max} in both directions had to be increased by a factor of 5.1. Alternatively, the K_m for 1,3GriP_2 (the most uncertain kinetic parameter for PGK) required adjustment by a factor of 0.75; the latter manipulation also changed the equilibrium constant. A change in the equilibrium constants therefore via alterations in the forward rate of Gra*P*DH and the K_m of 1,3GriP_2 for PGK, was the most effective way to match the *in vitro* kinetics with the *in vivo* behavior.

DISCUSSION

Comparison of models: different questions, different approaches

The approach in the existing models of yeast glycolysis, e.g [26–31] has been quite different from ours. In the biotechnological context, the model equations can be fitted to the experimental data concerning overall performance of the cell: the model is satisfactory if a good fit is obtained. This was the context of the modeling by Galazzo & Bailey [28], and Rizzi *et al*. [26]. The objective is a model that can describe the *in vivo* behavior, and predict this behavior under some other conditions. However, many rate equations, also mechanistically incorrect ones, may give good fits. Having the wrong rate equations however, increases the chance of erroneous prediction when the model is used outside the conditions used for fitting.

An alternative to fitting is to use the biochemical knowledge, gathered by *in vitro* kinetic studies, to predict the system behavior and then compare the prediction with experimental data. The prediction of the steady-state flux and the concentrations of the metabolites can be used to check whether the biochemical knowledge makes sense or not. This approach was successful for the relatively simple glycolytic pathway of *Trypanosoma brucei* [10], but less so for the much more complex TCA cycle of *Dictyostelium discoideum* [25].

In the impressive effort of modeling glycolysis in mammalian erythrocytes (e.g. [8,32–35]), the emphasis has been on developing a model that could satisfactorily describe erythrocyte glycolysis, rather than on the issue whether the pathway can be understood on the basis of kinetics determined *in vitro*. After all the isolated erythrocyte may be so atypical of living cells as to be unfit to address the question whether biochemistry can describe a living organism. Accordingly, linearized rather than realistic rate equations were used [8,32], most enzymes were treated as if at equilibrium [33], ATP, ADP, or NADH, NAD were treated as parameters [8,33], glucose transport was assumed to be at equilibrium [9,32–34], the values for kinetic parameters had not all been determined experimentally for the enzymes from the cognate source under the same *in vivo* conditions (e.g. [8,35]), or parameters were fitted so as to obtain optimum correspondence between model prediction and the experimental steady state properties [8,32,34,35]. The erythrocyte models have clarified issues which the present manuscript did not address. These included the development of a new theory of metabolic control [8,32], the description of metabolic disease [34], the description of glycolysis in the context of the much wider metabolic network it is part of [33] and the regulatory role of 2,3-bisphosphoglycerate [35].

In contrast to the other modeling studies, we used reversible kinetics for all but two enzymes (PFK and PDC). Because product insensitivity leads to diminished control by the enzymes downstream the product-insensitive enzyme even if there is still a feedback by cofactors to which the enzyme is sensitive [36,37], our inclusion of inhibition of PFK by F1,6bP_2, is an important improvement of the existing rate equations. During glycolytic oscillations, the concentration of F1,6bP_2 does oscillate in a range where PFK is sensitive to this product [16]. Moreover, our rate equation for PFK may be used when studying the effect of F2,6bP_2 metabolism on glycolysis, e.g. on its transition time during a transition from ethanol to glucose [38].

Another difference with most other models is that we (as did [26,27]) have treated the concentrations of NAD and NADH as free metabolic variables, as they may play an important role in the regulation of glycolysis. They certainly appear important in the regulation of the dynamics of yeast glycolysis, considering the important role of acetaldehyde in synchronizing glycolytic oscillations in populations of intact yeast cells [20,39–41]: Acetaldehyde most likely acts on these oscillations via the nicotine amide dinucleotides. When branching occurs, as it does (Table 1), the NADH/NAD ratio is important as it

mediates the constraint imposed on the glycerol and succinate branches by the redox balance requirement.

Finally, our approach has been different in that it has explicitly addressed the difficulty of combining and comparing kinetic parameters that have been measured under many different conditions, in different laboratories and from yeast which physiological state has not been specified. To tackle this problem, we have redetermined experimentally the kinetic parameters for most glycolytic enzymes under the same assay conditions and from the same source of yeast. Our set of kinetic parameters appears the most complete and consistent set among the existing glycolytic models.

Modeling as a heuristic tool: limits in our biochemical knowledge of glycolytic enzymes

The calculation of the adjustments that were required to fit the kinetics to the observed *in vivo* behavior, showed that no limited set of errors in enzyme parameters could be responsible for the discrepancy between model and experiment. The kinetics of all enzymes required adjustment, albeit to various degrees.

The kinetics of enzymes may be affected by many factors whose concentration differs between cell and assay. Moreover, unknown enzyme modifiers may exist which may change the apparent affinity constants significantly. Effective equilibrium constants may be affected by uncertainties in the exact activities of divalent cations (most notably Mg^{2+}), protons, phosphate and by differences in temperature (Our experiments were carried out at 30 °C whereas many equilibrium constants have been determined at 25 °C).

Most enzymes in the model required adjustments that appear reasonable given the uncertainties in extraction efficiency of both metabolites and enzymes, the exact conditions in the cytosol and errors in the determination of kinetic parameters. Some enzymes, however, showed larger discrepancies. The *in vitro* V_{max} of ADH appeared 10 times too high. One uncertainty may be the presence of isoenzymes of ADH. However, we estimated that ADH-I contributed to some 90% of the total activity of ADH, and used the kinetics for that isoenzyme in the model (see Appendix 1). A large proportion of NADH (and NAD) may be bound and not available to ADH. Moreover, our experiments did not discriminate between cytosolic and mitochondrial NADH. The latter may contribute significantly to the total NADH pool, especially because under anaerobic conditions the mitochondria may be expected to be reduced [42]. The steady-state concentration of NADH required to match the *in vitro* ADH kinetics with a concentration of acetaldehyde of 0.17 mM and the *in vivo* rate, was 0.04 mM, i.e. only 10% of the measured total concentration of NADH. Such a low free NADH concentration would also fit well with the Gra*P*DH kinetics. At 0.04 mM NADH, the concentration of Gra*P*DH would have to be increased by only a factor of 1.4, PGK remaining unchanged.

PDC required a sixfold increase in its maximal rate. Also Rizzi and colleagues reported on difficulties with this enzyme [26]. The affinity of PDC for pyruvate is known to depend on phosphate [43], but assuming a change in affinity alone did not lead to a match between *in vitro* flux and calculated rate (Table 5). Given its role in diverting the glycolytic flux into the direction of ethanol formation [44], it is not unlikely that PDC is regulated by other components that are as yet not known.

The *in vitro* activity of PGI was four times too low as compared to the *in vivo* rate. The measured kinetics fit reasonably well with the equilibrium constant via the Haldane relationship. The concentration ratio of G6*P* and F6*P* was close to the expected equilibrium ratio, i.e. [F6*P*]/[G6*P*] = 0.25, in agreement with earlier studies in resting yeast cells [45,46]. A similar discrepancy for PGI between the *in vitro* and *in vivo* activity was attributed to channeling between PGI and PFK, or regulation of PGI by unknown mechanisms [46].

Aldolase appeared to be too active *in vitro*. Although most studies agree on the K_m for F1,6bP_2 of the yeast enzyme [47–49], not much information was found on the inhibition of the enzyme by the products Gra*P* and glycerone phosphate. No data at all was found on the inhibitory constant of Gra*P* (K_{iq} in Eqn. A4); the value taken from Richter was an assumption only [27]. The value of K_{iq} that would fit with the *in vivo* data is about three orders of magnitude smaller than the one estimated by Richter. Complex formation of aldolase with G3*P*DH [50], Gra*P*DH [51] and PFK [52] has been suggested. Poly(ethylene glycol), a macromolecule enhancing macromolecular crowding, affected the association of aldolase with G3*P*DH, altering altered kinetic properties of the yeast aldolase [50].

Specific difficulties arose from the Gra*P*DH/PGK module being close to equilibrium. Although Gra*P*DH has been studied extensively, not many of its kinetic parameters have been measured under physiological conditions. Many studies were carried out at high pH where cooperative binding of NAD(H) is observed (reviewed in [53]). Moreover, the kinetics reported by Lambeir *et al.* [54], also used by us (except for the affinity for 1,3GriP_2, see Appendix 1), do not fulfill the Haldane relationship for the equilibrium constant. With our measured forward and backward maximal rates, the equilibrium constant calculated with the Haldane relationship was five times larger than the one measured by [54]. If the forward and reverse maximal rates from Lambeir *et al.* were used, the calculated equilibrium constant was even 75 times larger. For the kinetics of the glycosomal Gra*P*DH from *T. brucei*, this number was eight [54]. Thus, the kinetics of Gra*P*DH should be handled with caution.

PGK has been studied much more extensively under physiological conditions. Accordingly, the adjustments required for this enzyme are much smaller than for the Gra*P*DH enzyme. Considering the fact that the concentration of 1,3GriP_2 is not measurable, a phenomenological description of the Gra*P*DH-PGK module rate under a variety of product and substrate concentrations may suffice to model this step. Because the combined module is close to equilibrium, one may even be tempted to replace the module by an equilibrium pool, similar to what was performed for triosephosphate isomerase. However, one would then obscure a crucial feature of glycolysis: the thermodynamic hurdle of the Gra*P*DH reaction as a potential bottleneck of glycolysis (see below).

Impact of enzyme characteristics on the systemic behavior of the model

One property of one enzyme in the model has profound impact on the behavior of the whole system. This is the insensitivity of PFK for its carbon-derived product F1,6bP_2. Such a lack of product sensitivity impairs the signaling of a potential bottleneck in the ATP-producing steps of glycolysis [24,36,37]. When such a bottleneck was introduced during model development, that model exhibited accumulation of F1,6bP_2 (and downstream metabolites, depending on the site of the limitation),

at constant levels of cofactors and metabolites upstream PFK and downstream the bottleneck. This model behavior is reminiscent of the phenotype of the *tps1Δ* mutant [23]. Indeed, this 'phenotype' was not only seen in the first unbranched version of the model, but also when the glucose-transport activity was increased in the branched model (results not shown).

To prevent fructose-1,6-bisphosphate and downstream metabolites from accumulating, the rate of PFK should not exceed the capacity of the downstream reactions. This may be accomplished in many ways, of which two appear most relevant for anaerobic yeast glycolysis: limiting glucose uptake by the transporter, or introducing a brake on hexokinase via Tps1. Both should eventually lead to a decrease in the substrate for PFK, making the latter less active.

For many strains of *S. cerevisiae*, it is clear that the deletion of Tps1 leads to the lethal accumulation of F1,6bP_2 [23], and hence, that the inhibition on HK is of crucial importance. Our model did not include a Tps1-mediated feedback on hexokinase (only weak G6*P* inhibition was included). However, when such a strong feedback was included, the rate of hexokinase decreased, which led to an increased intracellular glucose concentration and hence, to reduced steady-state glucose transport activity (results not shown). Thus, the transport kinetics and steady-state glucose consumption rate as measured for the compressed yeast are incompatible with the presence of a strong feedback mechanism, via Tps1, acting on hexokinase. Moreover, it was remarkable that the V_{max} of glucose transport required a 20% increase to match the flux, as it is the only step that can be assayed directly *in vivo* in intact cells. Zero *trans* influx kinetic experiments have their limitations however, [55–57]: too low transport rates have been observed before [18,58] and constitute an unresolved problem in the field of glucose transport kinetics in yeast. It is therefore not unreasonable to assume that the actual transport capacity exceeds that measured by zero *trans* influx experiments. A model with increased transport capacity should allow a strong feedback on HK.

An increase in the activity of the processes that consume ATP, lumped into 'the ATPase', led to a *decrease* in the glycolytic flux (results not shown). A negative response of the glycolytic flux to the ATPase activity is unexpected in view of anaerobic glycolysis being the only source of ATP, but not ununderstandable [8,59]. This negative response in the model is caused by the positive effect of ATP on HK dominating the negative effects of ATP on PFK, PGK and PYK. When a strong inhibition on HK was added to the model (with a simultaneous increase in the limiting rate of glucose uptake to maintain the glycolytic flux), the glycolytic flux responded positively to a decrease in ATP, the inhibition of PFK by ATP then dominating (results not shown).

Regulation of hexokinase by Tps1 was absent from all other models described so far. One reason that those models did not show a *tps1-Δ* phenotype may be that the need for product inhibition of hexokinase was bypassed by supposed glucose 6-phosphate inhibition of the glucose transport step [26,30]. This may also have masked the impact of ignoring F1,6bP_2 sensitivity of PFK in these models. Our results highlight the implications of a Tps1-mediated feedback on hexokinase.

CONCLUSIONS AND PERSPECTIVES

The question addressed in the introduction, i.e. whether *in vitro* kinetics are able to describe *in vivo* behavior of a complicated metabolic pathway such as yeast glycolysis, does not have a simple answer. For half of the enzymes the *in vitro* kinetics did describe the *in vivo* activity satisfactorily, i.e. within a factor of two. For most of the enzymes that showed larger deviations, suggestions could be made that may have caused the discrepancy. This analysis may guide future experimentation that should lead to an improvement of our ability to understand the *in vivo* behavior of glycolysis on the basis of the properties of the glycolytic enzymes and their interactions. Once the uncertainties have been resolved by further rounds of experimentation and modeling, a tool is at hand with which not only pathway behavior may be described accurately, but which is then based on solid biochemical knowledge. It could then be used to explore the boundaries of metabolic engineering involving orders of magnitude changes in enzyme activities.

ACKNOWLEDGEMENTS

We would like to thank Peter Plomp and coworkers from DSM Bakery Ingredients for sharing kinetic data and experimental protocols and for providing us with the Koningsgist. We also acknowledge the financial assistance of the Netherlands Organization for Scientific Research (NWO), the European Union, and the Netherlands Association of Biotechnological Research Centers (ABON).

REFERENCES

1. Oliver, S.G. (1996) From DNA sequence to biological function. *Nature* **379**, 597–600.
2. Ovadi, J. & Srere, P.A. (1996) Metabolic consequences of enzyme interactions. *Cell Biochem. Funct* **14**, 249–258.
3. Srere, P.A. (1987) Complexes of sequential metabolic enzymes. *Annu. Rev. Biochem.* **56**, 89–124.
4. Kholodenko, B.N., Rohwer, J.M., Cascante, M. & Westerhoff, H.V. (1998) Subtleties in control by metabolic channeling and enzyme organization. *Mol Cell Biochem.* **184**, 311–320.
5. Rohwer, J.M., Postma, P.W., Kholodenko, B.N. & Westerhoff, H.V. (1998) Implications of macromolecular crowding for signal transduction and metabolite channeling. *Proc. Natl Acad. Sci. USA* **95**, 10547–10552.
6. Hofmeyr, J.-H.S., Kacser, H. & Van der Merwe, K.J. (1986) Metabolic control analysis of moiety conserved cycles. *Eur. J. Biochem.* **155**, 631–641.
7. Rapoport, T.A., Heinrich, R., Jacobasch, G. & Rapoport, S. (1974) A linear steady-state treatment on enzymatic chains. A mathematical model of glycolysis of human erythrocytes. *Eur. J. Biochem.* **42**, 107–120.
8. Heinrich, R., Rapoport, S.M. & Rapoport, T.A. (1977) Metabolic regulation and mathematical models. *Prog. Biophys. Mol Biol.* **32**, 1–82.
9. Westerhoff, H.V. & Van Dam, K. (1987) *Thermodynamics and Control of Biological Free-Energy Transduction.* Elsevier, Amsterdam, the Netherlands.
10. Bakker, B.M., Michels, P.A.M., Opperdoes, F.R. & Westerhoff, H.V. (1997) Glycolysis in bloodstream form *Trypanosoma brucei* can be understood in terms of the kinetics of the glycolytic enzymes. *J. Biol. Chem.* **272**, 3207–3215.
11. Sauro, H.M. & Fell, D.A. (1991) SCAMP: a metabolic simulator and control analysis program. *Math. Comp. Modelling* **15**, 15–28.
12. Walsh, M.C., Smits, H.P., Scholte, M. & Van Dam, K. (1994) The affinity of glucose transport in *Saccharomyces cerevisiae* is modulated during growth on glucose. *J. Bacteriol.* **176**, 953–958.
13. Lowry, O.H., Roseborough, N.J., Farr, A.L. & Randall, R.J. (1951) Protein measurement with the Folin phenol reagent. *J. Biol. Chem.* **193**, 265–275.
14. Bergmeyer, H.U. (1974) *Methods of Enzymatic Analysis.* Verlag Chemie, Weinheim, Germany.
15. De Koning, W. & Van Dam, K. (1992) A method for the determination

of changes of glycolytic metabolites in yeast on a subsecond time scale using extraction at neutral pH. *Anal. Biochem.* **204**, 118–123.
16. Richard, P., Teusink, B., Hemker, M.B., Van Dam, K. & Westerhoff, H.V. (1996) Sustained oscillations in free energy state and hexose phosphates in yeast. *Yeast* **12**, 731–740.
17. Theobald, U., Mailinger, W., Baltes, M., Rizzi, M. & Reuss, M. (1997) *In vivo* analysis of metabolic dynamics in *Saccharomyces cerevisiae*: I. experimental observations. *Biotechnol. Bioeng.* **55**, 305–316.
18. Teusink, B., Diderich, J.A., Van Dam, K., Westerhoff, H.V. & Walsh, M.C. (1998) Intracellular glucose concentration in derepressed yeast cells consuming glucose is high enough to reduce the glucose transport rate by 50%. *J. Bacteriol.* **180**, 556–562.
19. Parrou, J.L. & Francois, J. (1997) A simplified procedure for a rapid and reliable assay of both glycogen and trehalose in whole yeast cells. *Anal. Biochem.* **248**, 186–168.
20. Richard, P., Bakker, B., Teusink, B., Van Dam, K. & Westerhoff, H.V. (1996) Acetaldehyde mediates the synchronization of sustained glycolytic oscillations in yeast-cell populations. *Eur. J. Biochem.* **235**, 238–241.
21. Schulze, U., Liden, G., Nielsen, J. & Villadsen, J. (1996) Physiological effects of nitrogen starvation in an anaerobic batch culture of *Saccharomyces cerevisiae*. *Microbiol.* **142**, 2299–2310.
22. Gonzalez, M.I., Stucka, R., Blazquez, M.A., Feldmann, H. & Gancedo, C. (1992) Molecular cloning of CIF1, a yeast gene necessary for growth on glucose. *Yeast* **8**, 183–192.
23. Thevelein, J.M. & Hohmann, S. (1995) Trehalose synthase: guard to the gate of glycolysis in yeast? *Trends Biochem. Sci.* **20**, 3–10.
24. Teusink, B., Walsh, M.C., Van Dam, K. & Westerhoff, H.V. (1998) The danger of metabolic pathways with turbo design. *Trends Biochem. Sci.* **23**, 162–169.
25. Wright, B.E. & Albe, K.R. (1994) Carbohydrate metabolism in *Dictyostelium discoideum*: I. Model construction. *J. Theor. Biol.* **169**, 231–241.
26. Rizzi, M., Baltes, M., Theobald, U. & Reuss, M. (1997) *In vivo* analysis of metabolic dynamics in *Saccharomyces cerevisiae*: II. Mathematical model. *Biotechnol. Bioeng.* **55**, 592–608.
27. Richter, O., Betz, A. & Giersch, C. (1975) The response of oscillating glycolysis to perturbations in the NADH/NAD system: a comparison between experiments and a computer model. *Biosystems* **7**, 137–146.
28. Galazzo, J.L. & Bailey, J.E. (1990) Fermentation pathway kinetics and metabolic flux control in suspended and immobilized *Saccharomyces cerevisiae*. *Enz. Microbiol. Technol.* **12**, 162–172.
29. Cortassa, S. & Aon, M.A. (1994) Metabolic control analysis of glycolysis and branching to ethanol production in chemostat cultures of *Saccharomyces cerevisiae* under carbon, nitrogen or phosphate limitations. *Enz. Microbiol. Technol.* **16**, 761–770.
30. Cortassa, S. & Aon, M.A. (1997) Distributed control of the glycolytic flux in wild-type cells and catabolite repression mutants of *Saccharomyces cerevisiae* growing in carbon-limited chemostat cultures. *Enz. Microb. Technol.* **21**, 596–602.
31. Schlosser, P.M., Riedy, G. & Bailey, J.E. (1994) Ethanol production in Bakers' yeast: application of experimental perturbation techniques for model development and resultant changes in flux control analysis. *Biotechnol. Prog.* **10**, 141–154.
32. Rapoport, T.A., Heinrich, R. & Rapoport, S.M. (1976) The regulatory principles of glycolysis in erythrocytes *in vivo* and *in vitro*. A minimal comprehensive model describing steady states, quasi-steady states and time-dependent processes. *Biochem. J.* **154**, 449–469.
33. Joshi, A. & Palsson, B.O. (1990) Metabolic dynamics in the human red cell. Part III – Metabolic reaction rates. *J. Theor. Biol.* **142**, 41–68.
34. Holzhutter, H.G., Jacobasch, G. & Bisdorff, A. (1985) Mathematical modelling of metabolic pathways affected by an enzyme deficiency. A mathematical model of glycolysis in normal and pyruvate-kinase-deficient red blood cells. *Eur. J. Biochem.* **149**, 101–111.
35. Mulquiney, P.J. & Kuchel, P.W. (1999) Model of 2,3-bisphosphoglycerate metabolism in the human erythrocyte based on detailed enzyme kinetic equations: equations and parameter refinement. *Biochem. J.* **342**, 581–596.
36. Teusink, B., Mensonides, I.C., Bakker, B.M., Walsh, M.C., Snoep, J.L., Van Dam, K. & Westerhoff, H.V. (1998) Regulation through moiety conservation: the role of product sensitivity in glycolysis of yeast and trypanosomes. In *Biothermokinetics in the Post Genomic Era (*Larsson, C., Pahlman, I.-L.& Gustafsson, L., ed.), pp. 240–245. Chalmers Reproservice, Gothenburg, Germany.
37. Teusink, B. & Westerhoff, H.V. (2000) 'Slave' metabolites and enzymes. A rapid way of delineating metabolic control. *Eur J. Biochem.* **267**, 1889–1893.
38. Boles, E., Goehlmann, W.H. & Zimmermann, F.K. (1996) Cloning of a second gene encoding 6-phosphofructo-2-kinase in yeast, and its characterization of mutant strains without fructose-2,6-bisphosphate. *Mol. Microbiol.* **20**, 65–76.
39. Richard, P., Diderich, J.A., Bakker, B.M., Teusink, B., Van Dam, K. & Westerhoff, H.V. (1994) Yeast cells with a specific cellular make-up and an environment that removes acetaldehyde are prone to sustained glycolytic oscillations. *FEBS Lett.* **341**, 223–226.
40. Bier, M., Bakker, B.M. & Westerhoff, H.V. (2000) How yeast cells synchronize their glycolytic oscillations: a perturbation analytic treatment. *Biophys. J.* **78**, 1087–1093.
41. Wolf, J., Passarge, J., Somsen, O.J.G., Snoep, J.L., Heinrich, R. & Westerhoff, H.V. (2000) Transduction of intracellular and intercellular dynamics in yeast glycolytic oscillations. *Biophys. J.* **78**, 1145–1153.
42. Nissen, T.L., Schulze, U., Nielsen, J. & Villadsen, J. (1997) Flux distributions in anaerobic, glucose-limited continuous cultures of *Saccharomyces cerevisiae*. *Microbiol.* **143**, 203–218.
43. Boiteux, A. & Hess, B. (1970) Allosteric properties of yeast pyruvate decarboxylate. *FEBS Lett.* **9**, 293–296.
44. Pronk, J.T., Steensma, H.Y. & Van Dijken, J.P. (1996) Pyruvate metabolism in *Saccharomyces cerevisiae*. *Yeast* **12**, 1607–1633.
45. Wurster, B. & Schneider, F. (1970) Kinetik der Glucosephosphate-Isomerase (EC 5.3.1.9) aus Hefe und ihre Anwendung auf Flußberechnungen durch die Gärungkette anaeroben Hefezelle. *Hoppe-Seyler Z. Physiol. Chem.* **351**, 961–966.
46. Benevolensky, S.V., Clifton, D. & Fraenkel, D.G. (1994) The effect of increased PGI on glucose metabolism in *Saccharomyces cerevisiae*. *In situ* study of the glycolytic pathway in *Saccharomyces cerevisiae*. *J. Biol. Chem.* **269**, 4878–4882.
47. Banuelos, M. & Gancedo, C. (1978) *In situ* study of the glycolytic pathway in *Saccharomyces cerevisiae*. *Arch. Microbiol.* **117**, 197–201.
48. Midelfort, C.F., Gupta, R.K. & Rose, I.A. (1976) Fructose 1,6-bisphosphate: isomeric composition, kinetics, and substrate specificity for the aldolases. *Biochemistry* **15**, 2178–2185.
49. Richards, O.C. & Rutter, W.J. (1961) Comparative properties of yeast and muscle aldolase. *J. Biol. Chem.* **236**, 3185–3191.
50. Vertessy, B.G., Orosz, F. & Ovadi, J. (1991) Modulation of the interaction between aldolase and glycerol-phosphate dehydrogenase by fructose phosphates. *Biochim. Biophys. Acta* **1078**, 236–242.
51. Nuezil, J., Danielson, H., Welch, G.R. & Ovadi, J. (1990) Cooperative effect of fructose bisphosphate and glyceraldehyde-3-phosphate dehydrogenase on aldolase action. *Biochim. Biophys. Acta* **1037**, 307–312.
52. Tompa, P., Bar, J. & Batke, J. (1986) Interaction of enzymes involved in triosephosphate metabolism. Comparison of yeast and rabbit muscle cytoplasmic systems. *Eur. J. Biochem.* **159**, 117–124.
53. Harris, J.I. & Waters, M. (1982) Glyceraldehyde-3-phosphate dehydrogenase. In *The Enzymes* (Boyer, P.D., ed.), pp. 1–49. Academic Press, New York, USA.
54. Lambeir, A., Loiseau, A.M., Kuntz, F.M., Michels, P.M. & Opperdoes, F.R. (1991) The cytosolic and glycosomal glyceraldehyde 3-phosphate dehydrogenase from *Trypanosoma brucei*. *Eur. J. Biochem.* **198**, 429–435.
55. Walsh, M.C., Smits, H.P. & Van Dam, K. (1994) Respiratory inhibitors affect incorporation of glucose into *Saccharomyces*

cerevisiae cells, but not the activity of glucose transport. *Yeast* **10**, 1553–1558.

56. Smits, H.P., Smits, G.J., Postma, P.W., Walsh, M.C. & Van Dam, K. (1996) High-affinity glucose uptake in *Saccharomyces cerevisiae* is not dependent on the presence of glucose-phosphorylating enzymes. *Yeast* **12**, 438–447.
57. Teusink, B. (1999) *Exposing a Complex Metabolic System: Glycolysis in* Saccharomyces cerevisiae. PhD Thesis, University of Amsterdam, Amsterdam, the Netherlands.
58. Meijer, M.C.M., Boonstra, J., Verkleij, A.J. & Verrips, C.T. (1996) Kinetic analysis of hexose uptake in *Saccharomyces cerevisiae* cultivated in continuous culture. *Biochim. Biophys. Acta* **1277**, 209–216.
59. Heinrich, R. & Schuster, S. (1996) *The Regulation of Cellular Systems*, p. 187. Chapman & Hall, New York, USA.
60. Kotyk, A. (1967) Mobility of the free and of the loaded monosaccharide carrier in *Saccharomyces cerevisiae*. *Biochim. Biophys. Acta* **135**, 112–119.
61. Lang, J.M. & Cirillo, P. (1987) Glucose transport in a kinaseless *Saccharamyces cerevisiae* mutant. *J. Bacteriol.* **169**, 2932–2937.
62. Fuhrmann, G.F., Voelker, B., Sander, S. & Potthast, M. (1989) Kinetic analysis and simulation of glucose transport in plasma membrane vesicles of glucose-repressed and derepressed *Saccharomyces cerevisiae* cells. *Experientia* **45**, 1018–1023.
63. Kotyk, A. (1989) Kinetic Studies of transport in yeast. *Methods Enzymol.* **174**, 567–591.
64. Azam, F. & Kotyk, A. (1969) Glucose 6-phosphate as regulator of monosaccharide transport in bakers' yeast. *FEBS Lett.* **2**, 333–335.
65. Alonso, A., Pascual, C., Romay, C., Herrera, L. & Kotyk, A. (1989) Inhibition of hexose transport by glucose in a glucose-6-phosphate isomerase mutant of *Saccharomyces cerevisiae*. *Folia Microbiol. (Praha)* **34**, 273–278.
66. Rizzi, M., Theobald, U., Querfurth, E., Rohrhirsch, T., Baltes, M. & Reuss, M. (1996) *In vivo* investigation of glucose transport in *Saccharomyces cerevisiae*. *Biotech. Bioeng.* **49**, 316–327.
67. Perea, J. & Gancedo, G. (1978) Glucose transport in a glucose-phosphate isomeraseless mutant of *Saccharomyces cerevisiae*. *Curr. Microbiol.* **1**, 209–211.
68. Lobo, Z. & Maitra, P.K. (1977) Physiological role of glucose-phosphorylating enzymes in *Saccharomyces cerevisiae*. *Arch. Biochem. Biophys.* **182**, 639–645.
69. Viola, R.E., Raushel, F.M., Rendina, A.R. & Cleland, W.W. (1982) Substrate synergism and the kinetic mechanism of yeast hexokinase. *Biochemistry* **21**, 1295–1302.
70. Kopetzki, E. & Entian, K.-D. (1985) Glucose repression and hexokinase isoenzymes in yeast. *Eur. J. Biochem.* **146**, 657–662.
71. Hoggett, J.G. & Kellett, G.L. (1995) Kinetics of the cooperative binding of glucose to dimeric yeast hexokinase P-I. *Biochem. J.* **305**, 405–410.
72. De Winde, J.H., Crauwels, M., Hohmann, S., Thevelein, J.M. & Winderinckx, J. (1997) Differential requirement of the yeast sugar kinases for sugar sensing in establishing the catabolite-repressed state. *Eur. J. Biochem.* **241**, 633–643.
73. Blazquez, M.A., Lagunas, R., Gancedo, C. & Gancedo, J.M. (1993) Trehalose-6-phosphate, a new regulator of yeast glycolysis that inhibits hexokinase. *FEBS Lett.* **329**, 51–54.
74. Callens, M., Kuntz, D.A. & Opperdoes, F.R. (1991) Kinetic properties of fructose bisphosphate aldolase from *Trypanosoma brucei* compared to aldolase from rabbit muscle and *Staphylococcus aureus*. *Mol. Biochem. Parasitol.* **47**, 1–10.
75. Gozalbo, D., Gil-Navarro, I., Azorin, I., Renau-Piqueras, J., Martinez, J.P. & Gil, M.L. (1998) The cell wall-associated glyceraldehyde-3-phosphate dehydrogenase of *Candida albicans* is also a fibronectin and laminin binding protein. *Infect. Immun.* **66**, 2052–2059.
76. Singh, R. & Green, M.R. (1993) Sequence-specific binding of transfer RNA by glyceraldehyde-3-phosphate dehydrogenase. *Science* **259**, 365–368.
77. Ovadi, J., Bathe, J., Bartha, F. & Keleti, T. (1979) Effects of association-dissociation on the catalytic properties of GAPDH. *Arch. Biochem. Biophys.* **193**, 28–33.
78. Byers, L.D. (1982) Glyceraldehyde 3 phosphate dehydrogenase from yeast. *Methods Enzymol.* **89**, 326–335.
79. Ellenrieder, G.V., Kirschner, K. & Schuster, I. (1972) The binding of oxidized and reduced nicotinamide adenine dinucleotide to yeast glyceraldehyde-3-phosphate dehydrogenase. *Eur. J. Biochem.* **26**, 220–236.
80. Yang, S.T., Deal, J. & Deal, W.C. (1969) Metabolic control and structure of glycolytic enzymes. VI. Competitive inhibition of yeast glyceraldehyde-3-phosphate dehydrogenase by cyclic adenosine monophosphate, adenosine triphosphate, and other adenine-containing compounds. *Biochemistry* **8**, 2806–2813.
81. Byers, L.D., She, H.S. & Alayoff, A. (1979) Interaction of phosphate analogues with glyceraldehyde-3-phosphate dehydrogenase. *Biochemistry* **18**, 2471–2480.
82. Scopes, R.K. (1978) The steady-state kinetics of yeast phosphoglycerate kinase. *Eur. J. Biochem.* **85**, 503–516.
83. Mas, M.T., Resplandor, Z.E. & Riggs, A.D. (1987) Site-directed mutagenesis of glutamate-190 in the hinge region of yeast 3-phosphoglycerate kinase: implications for the mechanism of domain movement. *Biochemistry* **26**, 5369–5377.
84. Schmidt, P.P., Travers, F. & Barman, T. (1995) Transient and equilibrium kinetic studies on yeast 3-phosphoglycerate kinase. Evidence that an intermediate containing 1,3-bisphosphoglycerate accumulates in the steady state. *Biochemistry* **34**, 824–832.
85. Roustan, C., Brevet, A., Pradel, L.A. & Nguyen, V.T. (1973) Yeast 3-phosphoglycerate kinase. Interaction of enzyme with substrates studied by partial isotopic exchange and difference spectrophotometry. *Eur. J. Biochem.* **37**, 248–255.
86. Krietsch, W.K., Pentchev, P.G., Klingenburg, H., Hofstatter, T. & Bucher, T. (1970) The isolation and crystallization of yeast and rabbit liver triose phosphate isomerase and a comparative characterization with the rabbit muscle enzyme. *Eur. J. Biochem.* **14**, 289–300.
87. Schierbeck, B. & Larsson-Raznikiewicz, M. (1979) Product inhibition studies of yeast phosphoglycerate kinase evaluating properties of multiple substrate binding sites. *Biochim. Biophys. Acta* **568**, 195–204.
88. Grisolia, S. & Carreras, J. (1975) Phosphoglycerate mutase from yeast, chicken breast muscle, and kidney (2, 3-PGA-dependent). *Methods Enzymol.* **42**, 435–450.
89. White, M.F., Fothergill-Gilmore, L.A., Kelly, S.M. & Price, N.C. (1993) Dissociation of the tetrameric PGM from yeast by a mutation in the subunit contact region. *Biochem. J.* **295**, 743–748.
90. Gautan, N. (1988) Mutated forms of phosphoglycerate mutase affect reversal of metabolic flux. *J. Biol. Chem.* **263**, 15400–15406.
91. Entian, K.-D., Meurer, B., Koehler, H., Mann, K.-H. & Mecke, D. (1987) Studies on the regulation of enolases and compartmentation of cytosolic enzymes in *Saccharomyces cerevisiae*. *Biochim. Biophys. Acta* **923**, 214–221.
92. Hess, B., Haeckel, R. & Brand, K. (1966) FDP-activation of yeast pyruvate kinase. *Biochem. Biophys. Res. Comm.* **24**, 824–831.
93. Murcott, T.H., Gutfreund, H. & Muirhead, H. (1992) The cooperative binding of fructose-1,6-bisphosphate to yeast pyruvate kinase. *EMBO J.* **11**, 3811–3814.
94. Barwell, C.J. & Hess, B. (1972) Application of kinetics of yeast pyruvate kinase *in vitro* to calculation of glycolytic flux in the anaerobic yeast cell. *Hoppe-Seyler Z. Physiol. Chem.* **353**, 1178–1184.
95. McQuate, J.T. & Utter, M.F. (1959) Equilibrium and kinetic studies of the pyruvate kinase reaction. *J. Biol. Chem.* **234**, 2151–2157.
96. Yun, S.L., Aust., A.E. & Suelter, C.H. (1976) A revised preparation of yeast (*Saccharomyces cerevisiae*) pyruvate kinase. *J. Biol. Chem.* **251**, 124–128.
97. Johannes, K.J. & Hess, B. (1973) Allosteric kinetics of pyruvate kinase of *Saccharomyces carlsbergensis*. *J. Mol. Biol.* **76**, 181–205.
98. Wieker, H.J. & Hess, B. (1971) Allosteric interactions of yeast pyruvate kinase as a function of pH. *Biochemistry* **10**, 1243–1248.

99. Hunsley, J.R. & Suelter, C.H. (1969) Yeast pyruvate kinase. II. Kinetic properties. *J. Biol. Chem.* **244**, 4819–4822.
100. Macfarlane, N. & Ainsworth, S. (1972) A kinetic study of Bakers'-yeast pyruvate kinase activated by fructose 1,6-diphosphate. *Biochem. J.* **129**, 1035–1047.
101. Hubner, G., Weidhase, R. & Schellenberger, A. (1978) The mechanism of substrate activation of pyruvate decarboxylase: a first approach. *Eur. J. Biochem.* **92**, 175–181.
102. Ganzhorn, A.J., Green, D.W., Hershey, A.D., Gould, R.M. & Plapp, B.V. (1987) Kinetic characterization of yeast alcohol dehydrogenases. *J. Biol. Chem.* **262**, 3754–3761.
103. Wills, C. (1976) Production of yeast alcohol dehydrogenase isoenzymes by selection. *Nature* **261**, 26–29.
104. Wratten, C.C. & Cleland, W.W. (1963) Product inhibition studies on yeast and liver alcohol dehydrogenases. *Biochemistry* **2**, 935–941.
105. Buttgereit, F. & Brand, M.D. (1995) A hierarchy in ATP-consuming processes in mammalian cells. *Biochem. J.* **312**, 163–167.
106. Michnick, S., Dequin, S., Roustan, J.-L., Remize, F. & Barre, P. (1997) Modulation of glycerol and ethanol yields during alcoholic fermentation in *Saccharomyces cerevisiae* strains overexpressed or disrupted for *GPD1* encoding glycerol 3-phosphate dehydrogenase. *Yeast* **13**, 783–793.
107. Nevoigt, E. & Stahl, U. (1996) Reduced pyruvate decarboxylase and increased glycerol-3-phosphate dehydrogenase [NAD^+] levels enhance glycerol production in *Saccharomyces cerevisiae*. *Yeast* **12**, 1331–1337.
108. Blomberg, A. & Adler, L. (1989) Roles of glycerol and glycerol-3-phosphate dehydrogenase (NAD^+) in acquired osmotolerance of *Saccharomyces cerevisiae*. *J. Bacteriol.* **171**, 1087–1092.
109. Albertyn, J., Van Tonder, A. & Prior, B.A. (1992) Purification and characterization of G3PDH of *Saccharomyces cerevisiae*. *FEBS Lett.* **308**, 130–132.
110. Van Dijken, J.P. & Scheffers, W.A. (1986) Redox balances in the metabolism of sugar by yeasts. *FEMS Microbiol. Rev.* **32**, 199–224.
111. Otto, A., Przybylski, F., Nissler, K., Schellenberger, W. & Hofmann, E. (1986) Kinetic effects of fructose 1,6-bisphosphate on yeast phosphofructokinase. *Biomed. Biochim. Acta* **45**, 865–875.
112. Bartrons, R., Van Schaftingen, E. & Hers, H.G. (1982) The stimulation of yeast phosphofructokinase by fructose 2,6-bisphosphate. *FEBS Lett.* **143**, 137–140.
113. Przybylski, F., Otto, A., Nissler, K., Schellenberger, W. & Hofmann, E. (1985) Effects of fructose 1,6-bisphosphate on the activation of yeast phosphofructokinase by fructose 2,6-bisphosphate and AMP. *Biochim. Biophys. Acta* **831**, 350–352.
114. Hess, B. & Plesser, T. (1978) Temporal and spatial order in biochemical systems. *Ann. NY Acad. Sci.* **316**, 203–213.
115. Kessler, R., Schellenberger, W., Nissler, K. & Hofmann, E. (1988) Binding of fructose 2,6-bisphosphate to yeast phosphofructokinase. *Biomed. Biochim. Acta* **47**, 221–225.
116. Nissler, K., Otto, A., Schellenberger, W. & Hofmann, E. (1983) Similarity of activation of yeast phosphofructokinase by AMP and fructose 2,6-bisphosphate. *Biochem. Biophys. Res. Comm.* **111**, 294–300.
117. Bigl, M., Eschrich, K. & Hofmann, E. (1991) Kinetics of phosphofructokinase from a yeast mutant. *Biomed. Biochim. Acta* **50**, 239–250.
118. Fell, D.A. (1997) *Understanding the Control of Metabolism.* Portland Press, London, UK.
119. Kessler, R., Nissler, K., Schellenberger, W. & Hofmann, E. (1986) Binding of fructose-1,6-bisphosphate to yeast phosphofructokinase. *Biomed. Biochim. Acta* **45**, 1121–1125.
120. Stein, W.D. (1986) *Transport and Diffusion Across Cell Membranes.* Academic Press, London, UK.
121. Tewari, Y.B., Steckler, D.K. & Goldberg, R.N. (1988) Thermodynamics of isomerization reactions involving sugar phosphates. *J. Biol. Chem.* **263**, 3664–3669.
122. Hofmann, E. & Kopperschlaeger, G. (1982) Phosphofructokinase from yeast. *Methods Enzymol.* **90**, 49–60.
123. Burton, K. (1974) The enthalpy change for the reduction of nicotinamide-adenine dinucleotide. *Biochem. J.* **143**, 365–368.
124. Alberty, R.A. (1994) Biochemical thermodynamics. *Biochim. Biophys. Acta* **1207**, 1–11.

APPENDIX 1: ENZYME KINETICS

In this Appendix the rate equations, experimental kinetic data and an overview of the biochemical knowledge concerning the glycolytic enzymes are given. Derivations follow established practice [32,59]. One substrate, one product reversible Michaelis–Menten kinetics was used to describe the enzymes PGI, PGM and ENO:

$$v = V^{+}\frac{\frac{a}{K_a}\left(1-\frac{\Gamma}{K_{eq}}\right)}{1+\frac{a}{K_a}+\frac{p}{K_p}} \quad \text{(A1)}$$

where a and p represent the concentrations of the corresponding substrate and product, respectively. Γ is the mass-action ratio, p/a, K_{eq} is the equilibrium constant, p_{eq}/a_{eq}. K_a and K_p are the Michaelis–Menten constants for a and p. Reversible Michaelis–Menten kinetics for two noncompeting substrate-product couples was used for HK, Gra*P*DH, PGK and PYK:

$$v = V^{+}\frac{\frac{ab}{K_aK_b}\left(1-\frac{\Gamma}{K_{eq}}\right)}{\left(1+\frac{a}{K_a}+\frac{p}{K_p}\right)\left(1+\frac{b}{K_b}+\frac{q}{K_q}\right)} \quad \text{(A2)}$$

where a and b represent the concentrations of the substrates and p and q the concentrations of the products. For the other enzymes specific rate equations apply, as described in the following sections.

Transport of glucose: HXT

The transport of glucose across the cell membrane occurs via facilitated diffusion [56,60–62]. We have used a symmetrical carrier model:

$$v_{transport} = V^{+}\frac{\frac{[Glc_{out}]-[Glc_{in}]}{K_{Glc}}}{1+\frac{[Glc_{out}]}{K_{Glc}}+\frac{[Glc_{in}]}{K_{Glc}}+K_i\frac{[Glc_{out}]}{K_{Glc}}\frac{[Glc_{in}]}{K_{Glc}}} \quad \text{(A3)}$$

in which $[Glc_{out}]$ and $[Glc_{in}]$ are the concentrations of extracellular and intracellular glucose, respectively. The 'interactive constant' K_i depends on the relative mobility of the unbound and bound carrier [60,63], and was calculated in [18]. Despite the large number of transporters, glucose transport in derepressed yeast cells can be kinetically characterized by one high affinity component with a K_m of 1–2 mM [12]. This was also the case for the yeast used in this study: zero *trans*-influx of glucose occurred with a K_m of 1.2 mM (Table 2).

In the literature it has been proposed that glucose 6-phosphate inhibits glucose transport [64,65]. Such a feedback regulation has been incorporated in most of the glycolytic models [26,28–30,66]. The experimental basis for this feedback is controversial [67]. We have shown experimentally that, for high-affinity transport, the simplest model for a facilitated diffusion transporter (a symmetrical carrier whose rate depends on extra- and intracellular glucose only) can account for the difference between initial uptake rates and steady-state glucose consumption [18]. This removed the necessity of postulating inhibition by glucose 6-phosphate. This model has therefore also been used here.

Hexokinase: HK

In yeast three enzymes can phosphorylate glucose: hexokinase PI, hexokinase PII, and glucokinase [68]. In our glucose-derepressed compressed yeast, hexokinase PI appears to dominate: we found that $K_{mFru}/K_{mGlc} = 1.5$ and $V_{maxFru}/V_{maxGlu} = 2$ [68] (results not shown). Our K_m values for glucose and ATP agree well with published ones [47,68–70]. The kinetics of hexokinase appear more complicated than the simple Michaelis–Menten kinetics employed in this study. For example, binding of glucose enhances the affinity for ATP [69,71]. Such kinetics have not yet been incorporated. They may have implications for the role of glucose signaling by the hexokinases [72]. The impact of the more complex kinetics of hexokinase cannot be assessed yet, as data on the internal glucose concentration are yet lacking, and because product inhibition of the enzyme is not fully understood. Rather than being sensitive to its direct product, G6*P* (the K_i was estimated to be 40 mM), hexokinase appears negatively regulated, in an as yet unknown way, by trehalose 6-phosphate synthase [23]. Competitive inhibition by Tps1's metabolic product trehalose 6-phosphate may offer a mechanism [73]. In our model, as in all other published ones, no Tps1-mediated feedback mechanism was incorporated, as the feedback has not been characterized kinetically (see main text for the consequences).

Phosphoglucose isomerase: PGI

The kinetics of PGI have been measured in both directions and a reversible Michaelis–Menten equation was used to describe the kinetics of this enzyme. Our K_m values are in agreement with those found in the literature [45]. The kinetics fit reasonably well with the equilibrium constant ($K_{eq,PGI} = 0.31$) according to the Haldane relationship: we found an equilibrium constant of 0.26.

Aldolase: ALD

Aldolase is generally assumed to follow an ordered uni-bi mechanism, with Gra*P* binding after glycerone phosphate [27,74]. The equation is:

$$v_{ALD} = V^{+}\frac{\frac{a}{K_a}\left(1-\frac{\Gamma}{K_{eq}}\right)}{1+\frac{a}{K_a}+\frac{p}{K_p}+\frac{q}{K_q}+\frac{aq}{K_aK_{iq}}+\frac{pq}{K_pK_q}} \qquad \text{(A4)}$$

where a represents [F1,6bP_2], p represents [glycerone phosphate] and q represents [Gra*P*]. The kinetic parameters are scarce, but all agree on the K_m for F1,6bP_2: around 0.3 mM [47–49]. Not many studies have been performed on the backward reaction, the only numbers found were from [49]. Unknown is the inhibitory constant for Gra*P*: it was estimated by Richter [27] and used by others (including us), but experimental data is lacking.

Glyceraldehyde-3-phosphate dehydrogenase: GraPDH

The enzyme Gra*P*DH is an enigma. It is one of the most abundant enzymes in yeast [53]. In *S. cerevisiae*, it has been found in the cytosol and in the nucleus, and in some related yeast species it appears also located at the cell wall [75]. The enzyme appears to bind specific tRNAs [76].

The kinetics of the enzyme are renowned for their complexity. The enzyme forms monomers, dimers and tetramers that have different activities [77]. Cooperative binding of NAD and NADH has been documented well [53,78,79]. However, the cooperativity is only obvious at pH > 7.5 [78]. A complete data set of K_m values under conditions very similar to ours exists in the literature [54]; the authors did not observe cooperativity either. We have therefore not included cooperative binding in the rate equation, but rather used reversible two-substrates, two-products Michaelis–Menten kinetics. We have measured the V_{max} in either direction. Inhibition by the adenine nucleotides has been reported [80] and incorporated in some models [28,29], but the effects were very small with the inhibition constants and concentrations of the adenine nucleotides used in the model (result not shown). Therefore this inhibition has been left out.

When the Haldane relationship and our maximal rates and the affinities of Lambeir *et al*. [54] were used, the calculated equilibrium constant differed fivefold from the published equilibrium constant [81]. The most suspect parameter in the rate equation of Gra*P*DH is its affinity for 1,3GriP_2. 1,3GriP_2 was varied indirectly by *in situ* generation of 1,3GriP_2 by PGK, using excess 3Gri*P* and variable amounts of ATP. It was assumed that the ATP concentration added equaled the 1,3GriP_2 concentration at the excess of auxiliary enzyme added [54]. We have changed the uncertain K_m of 1,3GriP_2 (fivefold) so as to arrive at the known equilibrium constant for Gra*P*DH.

Phosphoglycerate kinase: PGK

PGK is difficult to assay in the forward direction because of the instability of its substrate, 1,3GriP_2. Many studies have been performed on the reverse reaction, however, with K_m values for 3Gri*P* in the range 0.2–0.5 mM [47,82–85], and for ATP between 0.1 and 0.5 mM [47,82–84,86]. Our values of 0.53 mM for 3Gri*P* and 0.3 mM for ATP agree with those. The K_m for 1,3GriP_2 was estimated by the K_i as measured by [87]. The K_m for ADP was taken from [86].

Phosphoglycerate mutase: PGM

PGM activity in yeast depends on 2,3-diphosphoglycerate. We have not taken 2,3GriP_2 into account, assuming that the enzyme is saturated with 2,3GriP_2. The K_m for 2,3GriP_2 is in the low micromolar range [88], whereas the concentration of 2,3GriP_2 was estimated to be 0.1 mM (result not shown). The K_m of PGM for its substrate 3Gri*P* differs considerably between studies. K_m values from 2 mM to 0.2 mM have been reported [47,88–90]. We measured and implemented a K_m value of 1.2 mM. For the product 2Gri*P*, a K_m value of 0.08 mM was used [90].

Enolase: ENO

Two isoenzymes of enolase are present in yeast. Class I enolase is expressed under glucose derepressed conditions; class II enolase is expressed during growth on glucose [91]. We measured a K_m value for 2Gri*P* that agrees well with that of class I enolase [91], in line with the derepressed state of the compressed yeast. Subsequently the K_m of the product phospho*enol*pyruvate was taken from class I enolase [91].

Pyruvate kinase: PYK

The most striking feature of pyruvate kinase is its strong activation by F1,6bP_2. At the low F1,6bP_2 concentrations prevailing during gluconeogenic conditions, the enzyme

showed cooperativity with respect to phospho*enol*pyruvate. At high F1,6bP_2 concentrations, however, the enzyme exhibited hyperbolic Michaelis–Menten kinetics with increased affinity for phospho*enol*pyruvate, in line with earlier findings [92,93]. We found that the activation is maximal at 0.5 mM of F1,6bP_2, which is more than 10 times lower than the concentration that we have measured. We have therefore used Michaelis–Menten kinetics. Our K_m values for phospho*enol*pyruvate and ADP fit well with the values found in numerous studies [47,92–99]. The affinities of the products are much less studied: we have equated them to the dissociation constants measured by Macfarlane and Ainsworth [100].

Pyruvate decarboxylase: PDC

Pyruvate decarboxylase exhibits cooperative kinetics with respect to its substrate pyruvate [43,101]. Irreversible Hill kinetics were used to describe this cooperativity:

$$v_{PDC} = V^{+}\frac{\left(\frac{[PYR]}{K_{0.5}}\right)^{n_H}}{1+\left(\frac{[PYR]}{K_{0.5}}\right)^{n_H}} \quad (A5)$$

The cooperativity and affinity for pyruvate are phosphate-dependent [43,101]. We have adopted the $K_{0.5}$ of 4.3 mM and the Hill coefficient of 1.9 as measured by Boiteux and Hess [43] at 25 mM phosphate. This $K_{0.5}$-value is in line with the 4 mM found by [47] (see also [44]).

Alcohol dehydrogenase: ADH

ADH follows ordered *bi-bi* kinetics, with the cofactor binding first [102]:

$$v_{ADH} = \frac{V^{+}\frac{ab}{K_{ia}K_b} - V^{-}\frac{pq}{K_pK_{iq}}}{1+\frac{a}{K_{ia}}+\frac{K_a b}{K_{ia}K_b}+\frac{K_q p}{K_pK_{iq}}+\frac{q}{K_{iq}}+\frac{ab}{K_{ia}K_b}+\frac{K_q ap}{K_{ia}K_pK_{iq}}}$$

$$+\frac{K_a bq}{K_{ia}K_bK_{iq}}+\frac{pq}{K_pK_{iq}}+\frac{abp}{K_{ia}K_bK_{ip}}+\frac{bpq}{K_{ia}K_bK_{iq}} \quad (A6)$$

where a is [ethanol], b is [NAD], p is [acetaldehyde] and q is [NADH].

Of the five isoenzymes of ADH present in yeast, ADH-I and ADH-II have clearly established metabolic functions. We estimated the contribution of ADH-I and ADH-II to the total ADH activity by varying the ethanol concentration and measuring the initial rate of NAD reduction in cell-free extracts. As the two enzymes differ in their affinity for ethanol by one order of magnitude (ADH-II having the higher affinity [102]), the two components were expected to be visible in this way. Indeed, Eadie–Hofstee plots of ADH activity vs. ethanol showed curved kinetics, indicative of more than one component. When two components were fitted, K_m values of 45 ± 10 and 0.7 ± 2 mM were found, with corresponding V_{max} values of 2.8 ± 0.2 and 0.3 ± 0.2 U·(mg total protein)$^{-1}$. Although the errors are substantial, especially in the high affinity component (corresponding to ADH-II), it can be concluded that the low-affinity component (corresponding to ADH-I) was the dominant isoenzyme under our conditions. It was checked that also the *in vitro* activity of ADH-I was tenfold higher than that of ADH-II when the measured metabolite levels (Table 1) were substituted in the rate equation for ADH. We have therefore used the kinetics of ADH-I only.

Kinetic parameters for ADH can be found in [102–104] We have chosen the data from Ganzhorn *et al*. as for each isoenzyme a complete data set including inhibition constants was given, under conditions very similar to ours [102]. The affinities for ethanol found by us are in reasonable agreement with the ones reported by Ganzhorn *et al*. ([102] 17 and 0.8 mM for ADH-I and ADH-II, respectively).

General ATPase

For glycolysis to proceed, the net ATP produced by PGK and PYK should be consumed by ATP consuming processes. These processes are lumped into one general ATPase, whose activity is set to be dependent on ATP, according to experimental observations [105]. A linear relation was used:

$$v_{ATPase} = k_{ATPase}\cdot[ATP] \quad (A7)$$

Branches of glycolysis

For simplicity, the fluxes to trehalose and glycogen were introduced as constants at the experimentally determined values. This is allowed because we here analyze one steady state. For further analysis, the substrate dependencies of these two branches will be required. For glycerol metabolism, it was assumed that glycerol 3-phosphate dehydrogenase completely controlled the flux through that pathway, as experimental evidence has shown that its control should be high [106–108]. Reversible Michaelis–Menten kinetics (Eqn. A3) were used, with glycerone phosphate and NADH as substrates and glycerol 3-phosphate and NAD as products. The glycerol 3-phosphate concentration was fixed at the measured value of 0.15 mM (Table 1).

The kinetics of G3*P*DH have not been studied extensively. We measured the affinity of G3*P*DH for glycerone phosphate, which was in agreement with that measured by Albertyn *et al*. [109]. Kinetic constants for NAD and NADH were from [109]. No data were found on the K_m of G3*P*DH to glycerol 3-phosphate. We have adopted a K_m value of 1 mM. The V_{max} of G3*P*DH turned out to be very sensitive to the salt and protein concentration in the assay, and no reliable V_{max} could be measured. Instead, we have adjusted the G3*P*DH V_{max} values to the measured glycerol flux.

The formation of glycerol leads to a redox imbalance in glycolysis, as NADH is oxidized in the process [110]. We have measured production of pyruvate, acetate and succinate. These weak carboxylic acids can account for 95% of the glycerol formation, with the production of succinate accounting for 80% of the glycerol production. For simplicity, we have only included a branch to succinate to counterbalance the glycerol branch. The origin of succinate is not clear; it can either be formed in the glyoxylate cycle or by part of the Krebs' cycle. As the latter involves both pyruvate and acetaldehyde as precursors and the former only acetaldehyde, we have chosen the glyoxylate cycle as the origin of succinate, for simplicity reasons only. As no kinetic data were available, the parameters had to be fit to the succinate production rate, and subsequently only stochiometric differences between the two alternative synthesis routes exist. The branch from acetaldehyde towards succinate via the glyoxylate cycle comprises many steps and was necessarily simplified by:

$$v_{succinate} = k_{succinate}\cdot[AcAld] \quad (A8)$$

APPENDIX 2: KINETICS OF PHOSPHOFRUCTOKINASE

PFK may be an enzymologists favorite, but it is a modelers nightmare. The difficulty is the many regulatory interactions and the resulting combinatorial explosion. Simplification is therefore required, and many effectors are necessarily assumed to be constant in the time window of the model, such as ammonium, phosphate, protons and fructose 2,6-bisphosphate. The regulatory effects that have been used explicitly in the existing glycolytic models are the cooperative binding of F6*P*, the inhibition by ATP (in some), the activation by AMP (in all, [26–29,66]) and ADP (only in [26]). The role of ADP in the regulation of PFK is much less important than those of ATP and AMP, and has not been included in our rate equation for PFK.

Product inhibition by F1,6bP_2 was not included in any of the existing models. The main inhibitory action of F1,6bP_2 is a decrease in the activation by F2,6bP_2 [111–113]. Therefore, a minimal kinetic model of PFK should be a function of the concentrations of F6*P*, ATP, AMP, F2,6bP_2 and F1,6bP_2. We have measured the activity of PFK in partially purified enzyme preparations as a function of F6*P* and ATP, and then looked at the effects of AMP and F2,6bP_2. The inhibitory effect of F1,6bP_2 was incorporated on the basis of data from Otto *et al*. [111]. To our knowledge, no model is available that describes all these effects at the same time. We have successfully tried to fit the same model as was used by Galazzo & Bailey [28], Schlosser *et al*. [31] and Cortassa & Aon [29]. It is based on the Monod, Wymann, Changeux model for allosteric enzymes, as adapted by Hess and Plesser [114] to apply to enzymes with two substrates.

The effect of AMP, F2,6bP_2 and F1,6bP_2, and the inhibitory effect of ATP are assumed to be mediated by displacement of the equilibrium between the Tense state and the Relaxed state, i.e. they affect the equilibrium constant L. It was assumed that the Tense state did not bind F6*P* and thus, that this state is inactive. The rate equation used to fit the *in vitro* kinetic data was therefore:

$$v_{\mathrm{PFK}} = V^{+}\frac{g_{\mathrm{R}}\lambda_1\lambda_2 R}{R^2 + LT^2} \tag{A9}$$

with:

$$\lambda_1 = [\mathrm{F6}P]/K_{\mathrm{R,F6}P} \tag{A10a, b}$$

$$\lambda_2 = [\mathrm{ATP}]/K_{\mathrm{R,ATP}}$$

$$R = 1 + \lambda_1\lambda_2 + g_{\mathrm{R}}\lambda_1\lambda_2 \tag{A11a, b}$$

$$T = 1 + c_{\mathrm{ATP}}\lambda_2$$

and:

$$L = L_0\left(\frac{1 + C_{\mathrm{i,ATP}}[\mathrm{ATP}]/K_{\mathrm{ATP}}}{1 + [\mathrm{ATP}]/K_{\mathrm{ATP}}}\right)^2 \cdot \left(\frac{1 + C_{\mathrm{i,AMP}}[\mathrm{AMP}]/K_{\mathrm{AMP}}}{1 + [\mathrm{AMP}]/K_{\mathrm{AMP}}}\right)^2 \tag{A12}$$

$$\left(\frac{1 + c_{\mathrm{i,F26b}P}[\mathrm{F26b}P]/K_{\mathrm{F26b}P} + c_{\mathrm{i,F16b}P}[\mathrm{F16b}P/K_{\mathrm{F16b}P}}{1 + [\mathrm{F26b}P]/K_{\mathrm{F26b}P} + [\mathrm{F16b}P]/K_{\mathrm{F16b}P}}\right)$$

The kinetic parameters for F6*P* and ATP were estimated by nonlinear regression of over our 200 experimental data points of the rate of PFK as a function of the concentrations of ATP and F6*P* [57]. Kinetic parameters are shown in Table 2. They are quite different from those used in the other models, most notably L_0 [28]. One reason may be that ATP inhibition was explicit in our equation, where it is implicit (and therefore ATP-independent) in the L_0 of the equation used by the other groups. If physiological ATP concentrations were substituted in the right hand side of Eqn. A12 (i.e. in the second factor in which ATP is involved), L increased by more than three orders of magnitude. Hofmann's group, however, have also found low L_0 values [115–117], in good agreement with ours.

Activation of AMP was measured at different F6*P* concentrations and at an ATP concentration of 1 mM [57]. These data were used to fit the binding parameters of AMP for the tense and relaxed state. The same procedure was followed for F2,6bP_2 activation [57]. F1,6bP_2 decreases the activation of F2,6bP_2, most probably by competition for the binding site. This can explain activation of PFK by F1,6bP_2 in the absence of F2,6bP_2 (results not shown; see [112,118]). Otto *et al.* showed an inhibition of F2,6bP_2 activation by F1,6bP_2 [111]. Their data was used to fit a model describing competition of F1,6bP_2 and F2,6bP_2 for the same site [57]. The same mechanism was used by Kessler *et al*. to describe the inhibitory effect of F1,6bP_2 on the activation by F2,6bP_2 [119]. A model of inhibition by F1,6bP_2 via competition with F6*P* could not describe the observed inhibition curves [57].

To our knowledge this is a first attempt to capture the effects of so many metabolites in a single rate equation. Our rate equation was able satisfactorily to describe the effects of the substrates F6*P* and ATP, the inhibition by ATP, the activation by AMP and F2,6bP_2 and the inhibitory effect of F1,6bP_2 on the activation by the latter.